JGR Oceans

RESEARCH ARTICLE
10.1029/2020JC016956

Growth and Decay of Northwestern Tropical Atlantic Barrier Layers

Aurpita Saha[1], Nuno Serra[1], and Detlef Stammer[1]

[1]Institute of Oceanography, Centrum für Erdsystemforschung und Nachhaltigkeit (CEN), Universität Hamburg, Hamburg, Germany

Key Points:

- The North Brazil and North Equatorial Currents are two regions with quasi-permanent barrier layers in the northwestern tropical Atlantic
- Large barrier layer thickness (BLT) within the rings occurs during June-July due to a thickening of the isothermal layer within the eddies
- Large winter BLT in North Equatorial Current is due to tilting of salinity fronts, stretching of isohalines, advection and turbulent mixing

Correspondence to:
A. Saha,
aurpita.saha@uni-hamburg.de

Citation:
Saha, A., Serra, N., & Stammer, D. (2021). Growth and decay of northwestern tropical Atlantic barrier layers. *Journal of Geophysical Research: Oceans*, *126*, e2020JC016956. https://doi.org/10.1029/2020JC016956

Received 5 NOV 2020
Accepted 21 MAR 2021

Abstract The growth and decay mechanisms of barrier layers in the northwestern tropical Atlantic are studied by investigating small-scale processes embedded in the regional circulation of the tropical Atlantic using output from an eddy-resolving numerical simulation at 4 km resolution forced by an atmospheric reanalysis. The simulation reproduces well the temporal and spatial patterns of barrier layer thickness (BLT) estimated with Argo and CTD in situ profiles. As seen from an analysis of the salinity and temperature vertical gradient balances, localized large barrier layers form inside North Brazil Current rings during late-June to July because of a thickening of the isothermal layer in the rings due to horizontal temperature advection, stretching of isotherms and tilting of temperature fronts. These barrier layers decay when the isothermal layer reduces again due to the above mechanisms. Further to the north, along the North Equatorial Current, the seasonal variability of BLT is highly pronounced. Thick winter (January to early March) barrier layers locally grow as the base of the mixed layer shoals mainly due to a tilting of the salinity fronts and partly due to stretching of the isohalines, horizontal salt advection and vertical turbulent mixing. The short-term barrier layers in this case decay due to a deepening of the mixed layer, whereas they get completely eroded in spring by a shoaling of the isothermal layer due to surface temperature stratification. This work highlights that barrier layers are localized phenomena at times growing solely due to ocean dynamics, without a surface freshwater influx.

Plain Language Summary Oceanic barrier layers exist in regions where salinity is more dominant than temperature in determining upper ocean density. Those layers lie between the bases of a constant-density layer and a constant-temperature layer. Barrier layers prevent vertical exchange of energy and mass between the near-surface and the deep ocean, thus influencing air-sea interaction. In the western tropical Atlantic, a warmer sea surface due to the presence of barrier layers can fuel hurricanes. Freshwater from the Amazon River and rainfall facilitate the growth of barrier layers, but the dynamics of their evolution are unclear. In this work, we identify/quantify the growth and decay mechanisms of barrier layers using a 4 km resolution simulation. Barrier layers grow/decay inside North Brazil Current eddies in summer because of deepening/shoaling of the constant-temperature layer inside the eddies due to horizontal heat transport. Further north, barrier layers grow in winter as the constant-density layer shoals mainly due to northwestward surface freshwater flow and equatorward subsurface salty water flow. Those barrier layers decay when the constant-density layer deepens, whereas are destroyed when the constant-temperature layer shoals in spring due to surface heating. These novel results improve the knowledge on barrier layers and help representing them in climate models.

1. Introduction

In the western tropical Atlantic, upper ocean temperature tends to be homogeneous from the surface down to the so-called "isothermal layer depth" (ILD) and salinity is responsible for density stratification. Freshwater discharge from the world's largest river, the Amazon (with an averaged annual discharge of about 0.2 Sv), precipitation under the Intertropical Convergence Zone (ITCZ) and several oceanographic processes induce a strong halocline (and therefore pycnocline) in the top few meters, leading to a "mixed layer depth" (MLD) that is shallower than the ILD (Balaguru, Chang, Saravanan, & Jang, 2012; Breugem et al., 2008; Masson & Delecluse, 2001; Mignot et al., 2007, 2012; Pailler et al., 1999; Sato et al., 2006; Silva et al., 2005; Sprintall & Tomczak, 1992). The thickness of the resulting "barrier layer" (BLT) is the difference between the ILD and the MLD.

Barrier layers are important as they prevent mixing between the thermocline and the mixed layer, thus diminishing the forcing of the thermocline by surface freshwater, heat and momentum fluxes, and enhancing their impacts on surface temperature and salinity. Furthermore, they also limit large effects of turbulent processes at the mixed layer base and prevent entrainment of cold water from the thermocline into the mixed layer (Drushka et al., 2014; Sprintall & Tomczak, 1992). As a consequence, the barrier layers can trap heat inside and above them, featuring a temperature inversion (Balaguru, Chang, Saravanan, & Jang, 2012; Mignot et al., 2012), thus increasing the sea surface temperature (SST) and causing potential intensification of tropical cyclones passing over the thick barrier layers (de Boyer Montégut et al., 2007; Balaguru, Chang, Saravanan, Leung, et al., 2012). Barrier layers therefore play a significant role in the upper ocean heat and salt budgets as well as in air-sea interaction (Vialard & Delecluse, 1998). They also affect currents by trapping momentum input from the wind in the shallow mixed layer, thereby producing strong surface flows (Drushka et al., 2014).

Located in the northwestern tropical Atlantic, the quasi-permanent barrier layers present throughout the year (Mignot et al., 2012) are likely more prominent and important than other barrier layers of the World Ocean (Foltz et al., 2004; Mignot et al., 2007, 2012). The thick barrier layers occurring within the Atlantic Warm Pool (AWP) in the northwestern tropical Atlantic are believed to originate primarily from advection of fresh Amazon and Orinoco river water and ITCZ precipitation, in combination with surface cooling during boreal fall and winter (Breugem et al., 2008; Mignot et al., 2012). The advection is maintained by the northwestward moving North Brazil Current (NBC) and associated rings (Ferry & Reverdin, 2004; Fratantoni & Glickson, 2002). Poleward transport of those fresh equatorial waters by the northward surface Ekman currents and equatorward sub-surface transport of Salinity Maximum Waters (SMW) may also contribute to the formation of barrier layers in this region (Balaguru, Chang, Saravanan, & Jang, 2012; Foltz et al., 2004; Mignot et al., 2007; Sato et al., 2006; Sprintall & Tomczak, 1992). Our study clarifies the relevance of all those mechanisms for the local barrier layer growth and decay. Henceforth, we address those barrier layers in the equatorial flank of the subtropical gyre as the barrier layers along the North Equatorial Current (NEC), as this is the dominant oceanic current there.

The seasonal cycle of BLT north of the Amazon mouth close to the equator is different from the seasonal cycle of BLT along the NEC in the northwestern tropical Atlantic. Masson and Delecluse (2001) studied the formation of barrier layers in the western tropical Atlantic (from 10°S to 10°N) by performing sensitivity experiments with an Ocean General Circulation Model. They explained that the temporal evolution of the sea surface salinity (SSS) is controlled by the dynamics: in summer the NBC and North Equatorial Countercurrent (NECC) systems advect the fresh water north- and northeastward and create large Amazon plumes three months after the Amazon flood in May-June. This creates thick barrier layers at the Amazon mouth from March to June (Silva et al., 2005) and in the north and east of the Amazon mouth from June to October (Masson & Delecluse, 2001; Pailler et al., 1999). Our study corroborates this finding and shows specifically that the NBC rings carry the conditions for barrier layer growth.

It is widely accepted that precipitation and river discharge are the main causes for the existence of barrier layers. However, ocean dynamics play a significant role in their formation, evolution and decay (Agarwal et al., 2012). Coles et al. (2013) using a 1°/6° HYCOM model and data from three research cruises (in May-June 2010, September-October 2011, and July 2012), identified four Amazon plume pathways of freshwater transport and found that the role of currents and advection is more important than river discharge in maintaining plume properties. In an analysis of Argo observations from January 2000 to June 2005, Sato et al. (2006) noticed patchy and thick barrier layer structures, which were explained by large-scale and small-scale (100 km) subduction processes in the subtropical gyres of the World Ocean. As those synoptic thick barrier layers appear in areas where the quasi-permanent climatological barrier layer is also thick, the climatological barrier layer is claimed to be a spatially and temporally smoothed picture of the synoptic barrier layers (de Boyer Montégut et al., 2007; Katsura & Sprintall, 2020; Mignot et al., 2007; Sato et al., 2006). According to the authors, since the Argo floats sample mesoscale features but do not resolve them, the role of mesoscale eddies to describe the barrier layer formation process needs to be assessed. In a study using the most recent Argo data on the formation mechanisms of barrier layers in the Southern Ocean, Pan et al. (2018) noted that, due to the lack of high resolution data, effects of mesoscale eddies and filaments, and the entrainment into barrier layers remain to be studied. This is a research gap that exists for most of

the barrier layers in the World Ocean, and is addressed in the present work for the above described northwestern tropical Atlantic barrier layers.

In some earlier modeling studies (Camara et al., 2015; Da-Allada et al., 2013; Ferry & Reverdin, 2004; Mignot et al., 2012; Sommer et al., 2015) and in a reanalysis and observational study (Foltz & McPhaden, 2008), the contribution of several processes to the salinity balance, which are responsible for the SSS changes in the tropical Atlantic, have been identified. But the processes that are responsible for the formation, evolution and decay of the barrier layers in this region have not been identified or defined before. Using the vertical derivative of salinity and temperature balance equations, Cronin and McPhaden (2002) provided the qualitative description of the relevant mechanisms by which barrier layers can form, grow and dissipate in the tropical Pacific under the influence of westerly wind bursts. A quantitative analysis was not possible in their case due to inadequate observational data. A qualitative or quantitative analysis of these mechanisms governing the evolution of barrier layers in the tropical Atlantic has not been performed yet, which leaves a large gap in the understanding of the growth and decay of these barrier layers. The present work aims at closing that gap.

The above findings motivate our study by highlighting the need for a better understanding and clarity of the mechanisms governing the generation, evolution and decay of the western tropical Atlantic barrier layers, especially those related to local circulation patterns and small-scale processes. The growth and decay of Atlantic barrier layers in the areas mentioned above in the tropical Atlantic is discussed in the present work in relation to ocean circulation features of the northwestern tropical Atlantic, such as the regional current systems (the NBC/NECC and the NEC), and certain other local processes (eddies and fronts). Along with temperature and salinity observations, output from an eddy-resolving simulation at 4 km resolution forced by fluxes computed with the ECMWF ERAinterim reanalysis facilitates our study of the finer details of the upper ocean dynamics.

The remaining study is structured as follows. Section 2 describes the model setup, the observational data sets and the methods employed. Section 3 presents the comparison of model and observations especially with regard to the seasonal variability of BLT. The governing mechanisms responsible for the growth and decay of barrier layers are identified and examined in two particular regions, the NBC rings area and the NEC region further to the north, in Sections 4 and 5, respectively. Section 6 provides a discussion and summarizes the main conclusions.

2. Data and Methods

2.1. Data

2.1.1. Atlantic Ocean Simulation

Our analyses are based on daily output from an integration of the Massachusetts Institute of Technology general circulation model (MITgcm) (Marshall et al., 1997) covering the Arctic Ocean and the Atlantic Ocean north of 33°S at 4 km horizontal resolution (henceforth termed ATL4km) for the period 2003–2011. The model was set up with a bipolar curvilinear grid, with one pole located over North America and the other over Europe. In the vertical, the model uses 100 layers of varying thickness, ranging from 5 m in the upper ocean to 185 m in the deep ocean. The model uses a z-coordinate vertical grid. Bottom topography is derived from the ETOPO 2-min resolution database. The model integration starts in year 2002 from initial conditions taken from an 8 km resolution 1948-present model integration, which in turn had initial conditions derived from the annual mean temperature and salinity from the World Ocean Atlas 2005 (Boyer et al., 2005). The vertical mixing parameterization employed in the simulations uses the KPP formulation. Background coefficients of vertical diffusion are set to 10^{-5} m^2/s and of vertical viscosity to 10^{-4} m^2/s. Horizontally, biharmonic diffusion and viscosity represent unresolved eddy mixing, with coefficients of horizontal diffusion and viscosity set to 1×10^9 m^4/s.

The model simulation is forced at the surface by fluxes of momentum, heat, and freshwater computed using bulk formulae and the 2002–2011 ECMWF ERA-Interim reanalysis (Dee et al., 2011). At the volume-balanced open northern and southern boundaries, the simulation is forced by the output of a 1° resolution global solution of the MITgcm forced by the NCEP reanalysis. A barotropic net inflow of 0.9 Sv

(1 Sv = 10^6 m^3/s) into the Arctic is prescribed at Bering Strait, the model's northern open boundary, which balances a corresponding outflow through the southern boundary at 33°S. A constant river runoff is applied at river mouths and a dynamic thermodynamic sea ice model solves for sea ice parameters.

Details about the model performance and previous validations against observations can be found in Serra et al. (2010), Köhl and Serra (2014), Koldunov et al. (2014), Sena Martins et al. (2015) and Biri et al. (2016).

2.1.2. Observational Data

The observational data set EN4.2.1 at 1° × 1° spatial resolution are used in our study. It is made available by the Met Office Hadley Center (https://www.metoffice.gov.uk/hadobs/en4). Both the observed subsurface ocean temperature and salinity individual profiles including data quality information and the monthly averaged objective analyzed fields (henceforth called EN4) are used. To make correct use of the profile data, the quality control flags indicating elimination of temperature and salinity observations due to vertical stability checks, track checks and vertical outlier checks were applied. Elimination of a profile was carried out if the profile is on the altimetry quality control suspect list, the profile appears to be on land, the profile is at exactly 0° latitude and longitude, the profile is on the Argo gray list, the profile is on the EN3 reject list, if there were no background values for this profile, or if over half its levels were rejected. Details of the quality control flags are given on the above website. Details of how the data set was constructed is provided in Good et al. (2013). The data set version with the Gouretski and Reseghetti (2010) bias correction applied is used in the present study.

In some comparisons, we additionally use the climatology of observed BLT (de Boyer Montégut et al., 2004), available from 1961 to 2008 at 2°× 2° spatial resolution from the IFREMER/LOS Mixed Layer Depth Climatology website (http://www.ifremer.fr/cerweb/deboyer/mld) (henceforth termed DeBoyer climatology).

2.2. Methods

2.2.1. Barrier Layer Thickness Computation

Following Sprintall and Tomczak (1992), de Boyer Montégut et al. (2004), de Boyer Montégut et al. (2007), Breugem et al. (2008), Mignot et al. (2012) and Drushka et al. (2014), we define ILD as the depth at which temperature has dropped by a value of ΔT = 0.2°C relative to the temperature at a reference depth of 2.5 m, the first depth level in the ATL4km simulation. MLD is defined as the depth at which potential density σ_θ has increased with respect to its value at the reference depth by an amount $\Delta\sigma_\theta$. Here $\Delta\sigma_\theta$ is the potential density change equivalent to the above temperature change at the local salinity:

$$\Delta\sigma_\theta = \sigma_\theta(T_{ref} - \Delta T, S_{ref}, P_0) - \sigma_\theta(T_{ref}, S_{ref}, P_0) \quad (1)$$

where T_{ref} and S_{ref} are the temperature and salinity at the 2.5 m reference depth and P_0 is the pressure at the ocean surface. The thickness of the BLT is defined as the positive difference between the ILD and the MLD:

$$BLT = ILD - MLD \quad for \quad ILD > MLD. \quad (2)$$

This definition of MLD ensures that, in the absence of haline stratification, that is, in the absence of barrier layers, the MLD and ILD are identical. Also, this definition of ILD takes care of temperature inversions that may be present in the barrier layer (Mignot et al., 2012).

2.2.2. Balance Equations and Governing Mechanisms

The growth and decay mechanisms of the barrier layers have not been quantified before in previous studies, though Cronin and McPhaden (2002) discuss these mechanisms qualitatively for the barrier layers in the western tropical Pacific. Our aim is to identify the mechanisms responsible for the growth and decay of the barrier layers in two localized regions of the northwestern tropical Atlantic, where large BLT is found: 1) in and around the NBC rings and 2) in the NEC. To understand how upper-ocean salinity/temperature stratification can develop in the northwestern tropical Atlantic, we computed the terms from the balance equations derived by Cronin and McPhaden (2002) using salinity, temperature, and the zonal, meridional and vertical components of velocity from daily averaged ATL4km model output. To study the growth and decay processes of upper ocean stratification and therefore of BLT, it is essential to have the four-dimensional

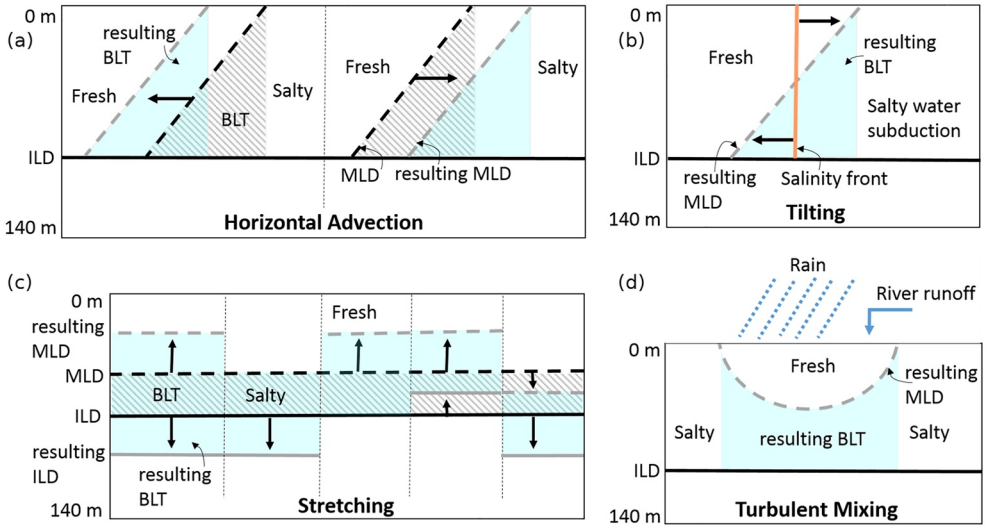

Figure 1. Schematics of (a) horizontal advection (term 1 in Equation 3), (b) tilting (term 3 in Equation 3), (c) stretching (term 4 in Equation 3) and (d) turbulent mixing (term 5 in Equation 3), the mechanisms responsible for barrier layer formation and growth. The black and gray dashed lines are, respectively, the initial and the resulting mixed layer depth (MLD). The black and gray solid lines depict, respectively, the initial and the resulting isothermal layer depth (ILD). Hatched regions are the initial barrier layers and the blue shaded regions depict the resulting barrier layers. Adapted and expanded from Cronin and McPhaden (2002).

fields of the above variables. Following Cronin and McPhaden (2002), the vertical derivative of the salinity balance equation is:

$$\frac{\partial}{\partial z}\left(\frac{\partial S}{\partial t}\right) = \underset{1}{-U\cdot\frac{\partial}{\partial z}(\nabla S)} \quad \underset{2}{-w\frac{\partial^2 S}{\partial z^2}} \quad \underset{3}{-\frac{\partial U}{\partial z}\cdot\nabla S} \quad \underset{4}{-\frac{\partial w}{\partial z}\frac{\partial S}{\partial z}} \quad \underset{5}{-\frac{\partial^2(\overline{w'S'})}{\partial z^2}}. \tag{3}$$

The vertical derivative of the temperature balance equation is:

$$\frac{\partial}{\partial z}\left(\frac{\partial T}{\partial t}\right) = \underset{1}{-U\cdot\frac{\partial}{\partial z}(\nabla T)} \quad \underset{2}{-w\frac{\partial^2 T}{\partial z^2}} \quad \underset{3}{-\frac{\partial U}{\partial z}\cdot\nabla T} \quad \underset{4}{-\frac{\partial w}{\partial z}\frac{\partial T}{\partial z}} \quad \underset{5}{-\frac{\partial^2(\overline{w'T'})}{\partial z^2}} \quad \underset{6}{+\frac{1}{\rho c_p}\frac{\partial^2 Q_{rad}}{\partial z^2}}. \tag{4}$$

In the above equations, S is the salinity, T is the temperature, $U = (u, v)$ is the horizontal velocity, w is the vertical velocity, z is the depth and $\overline{w'S'}$ and $\overline{w'T'}$ are the vertical turbulent fluxes of salinity and temperature, respectively. At the air-sea interface ($z = 0$) the turbulent salinity flux depends on the surface freshwater forcing by precipitation (P), evaporation (E) and river runoff (R):

$$(\overline{w'S'})\,|_{z=0} = S_0(P - E + R) \tag{5}$$

where S_0 is the surface salinity. The surface forcing is thus contained in the turbulent mixing component (term 5 in the right hand side (RHS) of Equation 3). In Equation 4, ρc_p is the volumetric heat capacity, Q_{rad} is the penetrative solar radiation, and $\overline{w'T'}$ at $z = 0$ is proportional to the net surface heat flux reduced by the solar radiation at the surface.

Each RHS term of the balance equations corresponds to a physical mechanism. Term 1 is the contribution to the tendency (either of salinity or temperature stratification) from horizontal advection. If favorable T/S conditions are advected leading to a "translation" of the MLD with constant ILD, a local change will be noticed by a thickening of the barrier layer in the flow direction (Figure 1a). A barrier layer can also form when a vertically sheared horizontal flow advects a horizontal salinity gradient within the isothermal surface layer (term 3, termed tilting). This causes near-vertical isohalines to tilt into the horizontal, thus forming a shallow mixed layer on top of the isothermal layer (Figure 1b). Vertical advection (term 2) acting uniformly on both the MLD and ILD will cause the barrier layer to shift vertically, with no change in BLT.

Thus this term is not implicated in the formation/evolution of barrier layers. But if the vertical velocity acts non-uniformly on the MLD and ILD surfaces, then the barrier layer can grow through vertical stretching (term 4, Figure 1c). Finally, rainfall (and/or river discharge) in the absence of strong turbulent mixing and surface heating, can cause a barrier layer to form between the base of the rainwater puddle (fresh lens) and the top of the ILD (term 5, Figure 1d).

The above four mechanisms lead to the formation and growth of barrier layers. These barrier layers decay when the same above mechanisms act in an opposite manner. Therefore, the T/S conditions forming a barrier layer can be advected away from a location and the T/S conditions unfavorable for the existence of barrier layers can be advected to that place. The tilting of a strong vertical salinity gradient (a horizontal front) that exists in presence of barrier layer can get tilted to form a horizontal salinity gradient (i.e., tilted into a vertical front) thus decaying the BLT. In order to reduce the BLT, the vertical velocities shown in the five cases of stretching in Figure 1c would have a reversed direction (in all five cases) and opposite magnitudes (in the cases when the different magnitudes of velocities act on both the surfaces, two right-most cases in Figure 1c). A strong turbulent mixing of saline and cold water from greater depths can destroy the BLT and turbulent mixing of warm water on the surface can also destroy the BLT.

Area averages of simulated BLT were computed in two regions: 1) the area where NBC rings form and propagate and 2) the area of the NEC. The events showing a strong peak in the resulting daily time series were chosen and the mechanisms contributing to the growth and decay of each of those barrier layers were examined in detail. To study the relation between barrier layers and NBC rings, the NBC rings were identified in the daily model output with the help of the Okubo-Weiss parameter (Chelton et al., 2011; Isern-Fontanet et al., 2004). In the region of NBC rings and for each event, an average of T/S properties and of the balance terms were taken over a period of 3 days before the event and compared with those at the time of peak BLT to understand the formation/thickening of the barrier layers. Conversely, averages over 3 days after the peak BLT were used to understand the barrier layer destruction/thinning. For the NEC events, the same procedure was conducted, averaging over periods of 3–5 days (chosen depending on the changes seen in the daily BLT) before and after the day showing the peak BLT. Those averaging periods correspond to half the duration of the respective barrier layer growth + decay event.

The salinity and temperature vertical gradients $\left(\frac{\partial S}{\partial z}\right), \left(\frac{\partial T}{\partial z}\right)$ were also examined along with the behavior of the isohalines and isotherms. The relative contribution of salinity and temperature to stratification was found by decomposing the squared Brunt-Väisälä frequency (N^2) as a sum of haline (N_S^2) and thermal (N_T^2) contributions, that is, $N^2 = N_S^2 + N_T^2 \equiv -\frac{g}{\rho}\frac{\partial \rho}{\partial z} = -g\beta\frac{\partial S}{\partial z} + g\alpha\frac{\partial T}{\partial z}$, where β is the haline contraction coefficient, α is the thermal expansion coefficient, g is the acceleration due to gravity and ρ is the density (Maes & O'Kane, 2014).

3. Comparison Between Observed and Simulated Barrier Layers

From comparisons with published work (Fonseca et al., 2004; Fratantoni et al., 2000; Schott et al., 1998; Stramma et al., 2005), the major regional circulation features of the tropical north Atlantic, such as the NEC, the NBC, and the NECC were seen to be well reproduced in the model. As Figure 2 illustrates, the simulated NBC advects the mixed layer properties (salinity in this case) toward the northwest throughout the year. The properties are transported toward the east in summer and fall by the NECC, starting in May-June and persisting until December. A component to the north of this transport of properties is insured by the prevailing Ekman transport.

As previously shown in Biri et al. (2016), the ATL4km model simulates well the observed patterns of eddy kinetic energy. The eddy activity related to the NBC is also realistic in the simulation, with about seven large rings being formed per year from the NBC retroflection. All this gives us confidence in using the model to correlate the variability of barrier layers with ocean dynamical features.

The average BLT computed from monthly EN4 temperature and salinity profiles and EN4 objective analyzed fields is here compared with the BLT computed from daily and monthly ATL4km output. Selected

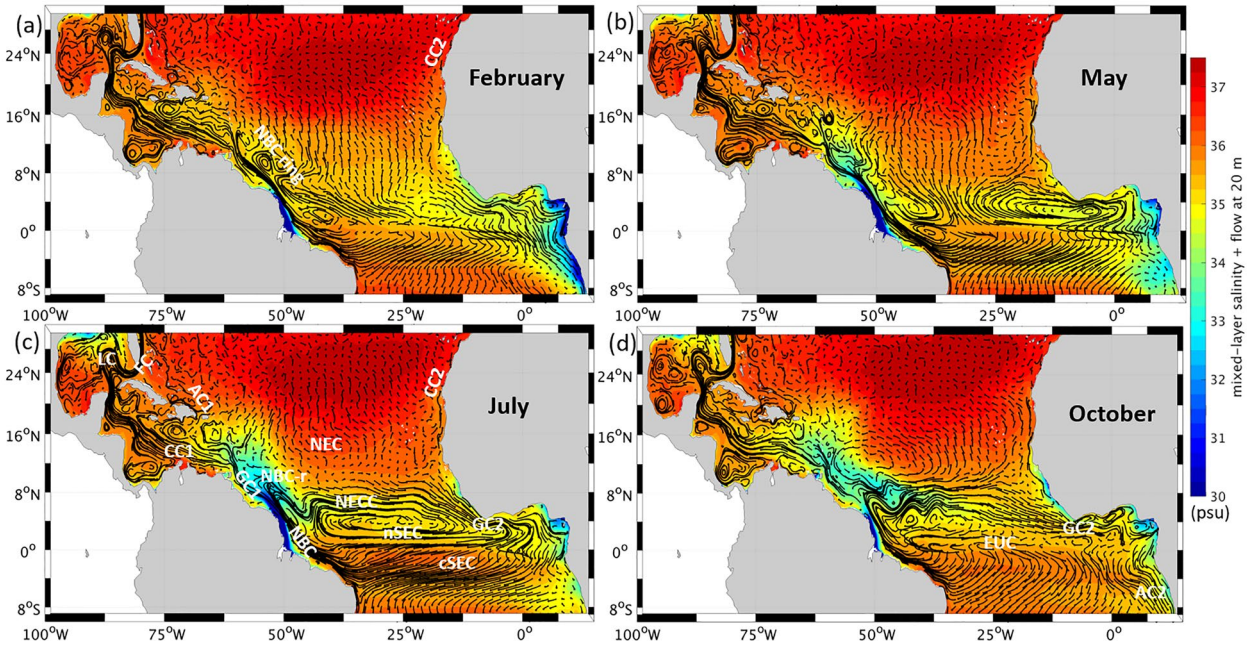

Figure 2. Climatology of simulated mixed-layer salinity and simulated flow at 20 m depth for the months of (a) February, (b) May, (c) July, and (d) October. The flow trajectories result from a 30-days integration of particles using the climatological three-dimensional ocean velocity of the respective month. Labeled are the North Brazil Current (NBC), the North Brazil Current retroflection (NBC-r), the North Equatorial Countercurrent (NECC), a North Brazil Current ring (NBC ring), the Guiana Current (GC1), the Caribbean Current (CC1), the Loop Current (LC), the Florida Current (FC), the Antilles Current (AC1), the North Equatorial Current (NEC), the Canary Current (CC2), the Guinea Current (GC2), the South Equatorial Current (SEC) with the northern (nSEC) and central (cSEC) branches, the Equatorial Undercurrent (EUC) and the Angola Current (AC2).

months from climatological averages are shown in Figure 3. In the case of the model, the number of days that a barrier layer was present in that given month is shown in the last respective panel (Figures 3d, 3h, 3l, and 3p) as an average over the 9-years period. This helps locate the places where barrier layers are of common occurrence in the model.

The northwestern tropical Atlantic is the region with largest barrier layer coverage almost throughout the year. The ATL4km simulation and the EN4 analyzed fields show similar spatial patterns in the distribution of BLT, but there are some large differences as well. Maximum spatial coverage in the northwestern tropical Atlantic occurs in February (Figures 3a–3d) and minimum in May (Figures 3e–3h).

Overall, EN4 has larger BLT than the simulation. Since spurious barrier layers could be generated by spatial and temporal interpolation of the sparsely available temperature and salinity profiles, the individual in situ profiles are used here to validate the BLT found in the EN4 and in the model. BLT computed from available Argo and CTD individual profiles of temperature and salinity show that barrier layers are a very localized phenomenon. The sparsely observed (in space and time) BLT distribution (Figures 3b, 3f, 3j, and 3n) is consistent with the results from the simulation and other data sets, but not enough profiles are available for a detailed comparison for each month in the period 2003–2011. Due to the small amount of data, it is not clear if the visible discrepancy in barrier layer spatial coverage between model and the EN4 analyzed fields is due to model deficiencies or due to interpolation of in situ profiles to regions with no information. Indeed, the EN4 results should be interpreted with some care. In fact, some signals seen in EN4-derived BLT have no correspondence in the profiles that serve as basis for the objective analysis. Studies suggest that interpolation of in situ profile data in gridded data sets creates BLT artifacts (de Boyer Montégut et al., 2007; Katsura & Sprintall, 2020; Mignot et al., 2007; Sato et al., 2006). We take therefore the EN4 results as being only illustrative rather than giving true BLT amplitudes. We conclude that the results from the profiles give a closer look at what has been observed regarding barrier layers. The results from the profiles indicate that coherence of barrier layers is less than what the EN4 analysis shows. When taking only the profiles into account, the model BLT amplitude and spatial variability seem realistic.

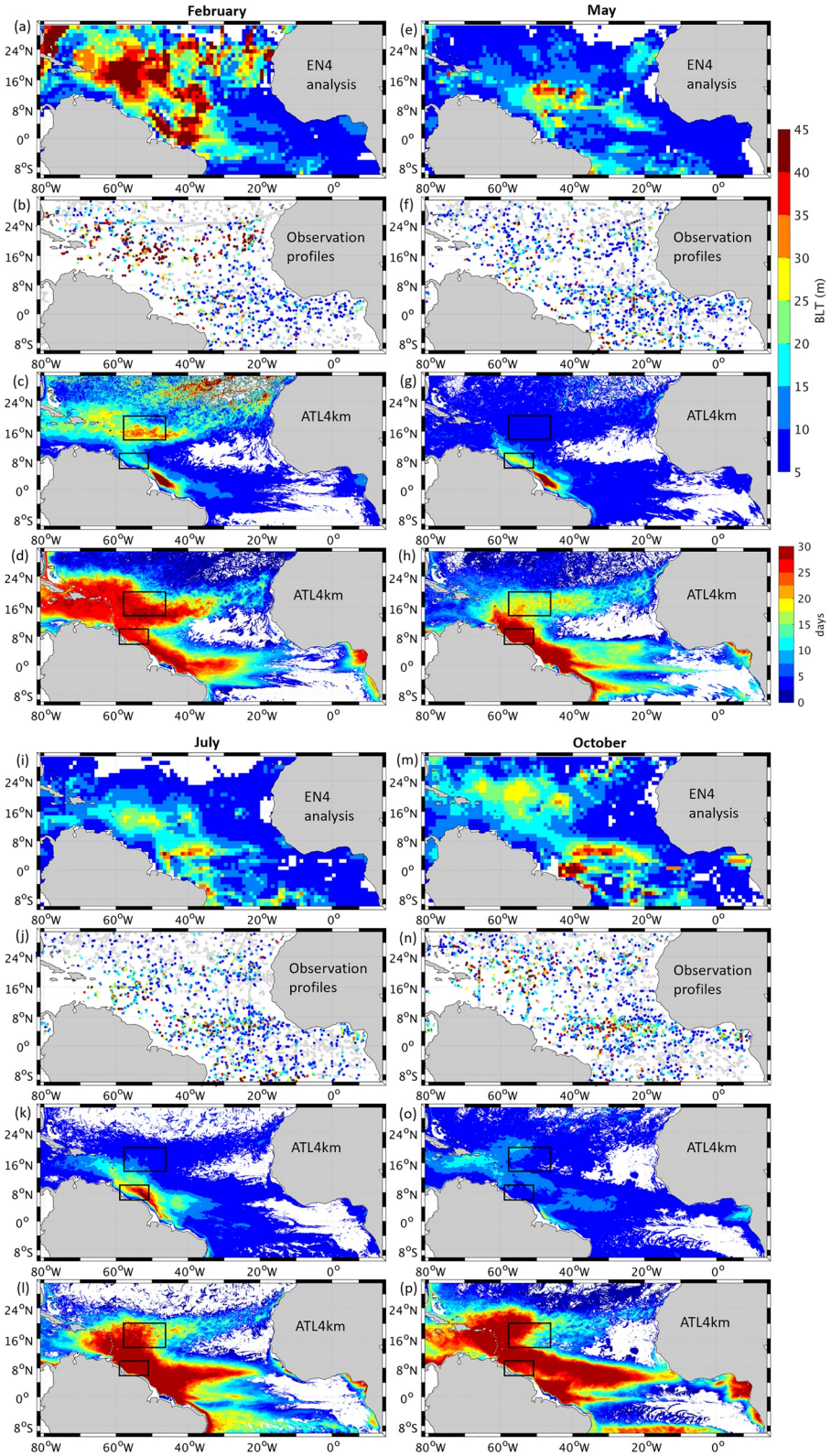

Figure 3. Spatial variability of BLT (meters) in February (top-left), May (top-right), July (bottom-left) and October (bottom-right) computed from monthly EN4 objective analyzed fields (a,e,i,m), in situ profiles (b,f,j,n) and ATL4km daily model output (c,g,k,o). The average number of days positive BLT was present in the period 2003–2011 is shown (d,h,l,p). The black boxes delimit the areas of large BLT studied in the present work: Southern box (6°N–10°N, 51°W–59°W) and northern box (14°N–20°N, 46°W–58°W). BLT, barrier layer thickness.

During February BLT goes up to 75 m in EN4 and up to 55 m in the DeBoyer climatology (not shown) and in ATL4km. Compared to the other data sets, EN4 has a larger spatial coverage of high BLT than the simulation. The reason for this is a deeper simulated winter mixed layer compared to observations, what could be attributed to unrealistic forcing or to missing/unresolved mixed layer processes in the model. During February (and in general during winter), the model generates barrier layers mostly at the Amazon mouth region and further north along the NEC and Antilles Current (AC1) (Figure 3c, currents in Figure 2c). The reasons for the growth and decay of those latter barrier layers (northern black NEC-box) will be explored in Section 5. Between the two regions, there is a stripe of moderately large BLT (southern black NBC-box), which the model shows being supported by the presence of NBC eddies. That BLT signal is investigated in Section 4.

In May, BLT is only up to 35 m in EN4 in the northwestern tropical Atlantic and most of the signal along the NEC and AC1 is not present. On the other hand, during May, maximum Amazon discharge near the coast gives rise to a freshwater plume there with consequent large barrier layers, as seen in the simulation. The large signal in the region adjacent to the Amazon mouth is not visible in the EN4 analysis, however, when inspecting the actual in situ profiles, large BLT is seen in the locations pointed by the model.

During July (Figures 3i–3l), the discharged Amazon freshwater spreads northwestward and eastward, leading to barrier layers being present 1) along the eastern limb of the Amazon plume and 2) further north to the east of the Lesser Antilles. This is due to the presence of the NECC, bringing the Amazon low salinity water into the ocean interior. The model reproduces this tendency seen in the observations. The model presents still a strong BLT signal offshore of the Amazon mouth (6°N–10°N, 51°W–59°W NBC-box), not seen in the EN4 analysis. However, there are a few profiles with barrier layers in that region during the months of May and July (Figures 3f and 3j).

In October, the BLT distribution from the EN4 analysis resembles still the one in July, with a further intensification along the NECC and the emergence of large BLT north of 16°N, a region which is building in importance toward winter. The model BLT distribution for October shows the largest amplitude discrepancy compared with EN4 profiles, with the model underestimating the observed BLT. Still, a tendency is seen toward increasing BLT in the northern NEC-box.

The model provides, however, more details than the observations about the spatial variability of barrier layers. Judging by the number of days per month with barrier layers (Figures 3d, 3h, 3l, and 3p), it is concluded that barrier layer formation is a common feature, albeit most of the times with small amplitudes. In those frequency distributions, it is seen how the winter (February) barrier layers are frequent in the Lesser and Greater Antilles regions and how they extend along the NEC and along the equator. In spring (May), the equatorial and off-equatorial currents show barrier layer formation, with the NEC region losing importance. In summer (July), the large impact of the NECC and of NBC eddies (more on this in Section 4) is seen, making barrier layers frequent at the southern NBC-box, along the NECC and east of the Lesser Antilles. That tendency continues through the fall (October), until the NEC region starts to develop large barrier layers again.

As seen in the simulation, barrier layer formation is a highly variable phenomenon, sometimes made up of sporadic events. Therefore, an average over the whole time series is not a good indicator of typical BLT, since a barrier layer absence will bias locally the mean BLT estimate toward zero. In Figure 4, a time average of BLT which is over 2 standard deviations of the local time series is presented. The regions where large barrier layers form are now more visible. At all months except November, the model forms large barrier layers in the region immediately adjacent to the Amazon mouth. In February there are large barrier layers occurring to the north of 12°N (Figure 4a), but only around 16°N are they often forming (Figure 4b). In May, large BLT (>25 m) is mostly confined to the South American coast (Figure 4c). In July, the region of large BLT extends toward the Caribbean Sea and to the east along the NECC (Figure 4e). The frequency of occurrence plot for July illustrates in particular the latter extension (Figure 4f). During October, the Caribbean Sea remains with large BLT and the NECC region fades compared to July (Figure 4g). The pattern of occurrence in October shows a shift to the north, but corresponds only to more moderate barrier layers (Figure 4h). It can also be noticed that the southern box area indeed shows large barrier layers most of the year; however, they are only present less than 15 days in an average month. Comparing with Figure 3, the BLT values in

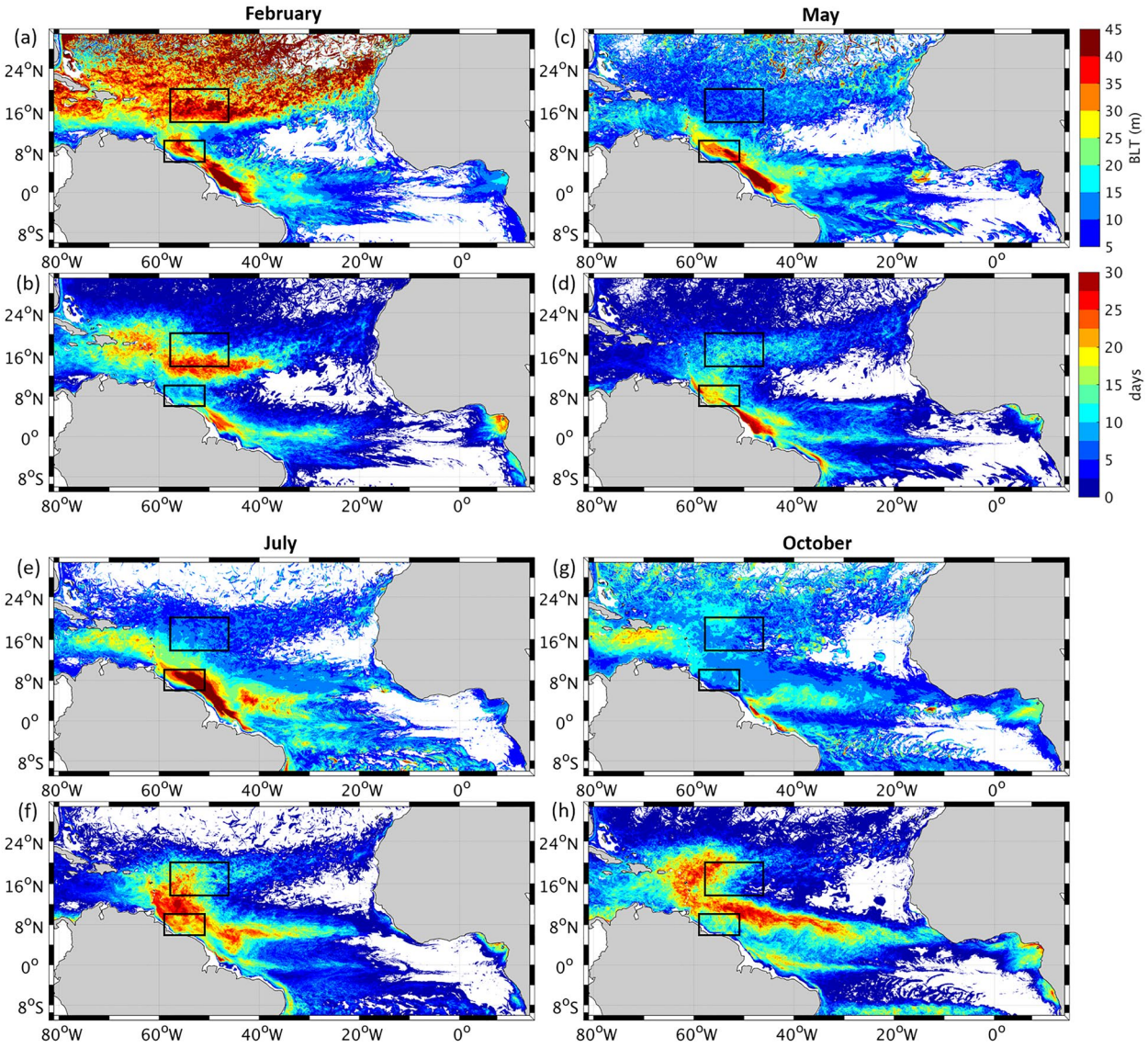

Figure 4. Spatial variability of the largest simulated BLT (average over 2 standard deviations) in February (top-left), May (top-right), July (bottom-left) and October (bottom-right). The corresponding average number of days in the period 2003–2011 is shown in (b,d,f,h). BLT, barrier layer thickness.

Figure 4 better approach the ones from observations, probably suggesting that a large under sampling is present in the observational estimate.

There are two localized regions in the northwestern tropical Atlantic which have large BLT peaking in different months. These are enclosed in the two small boxes in Figures 3 and 4 and will be further discussed in this work. In the northern NEC-box (14°N–20°N, 46°W–58°W) BLT is large in the months December-March, with largest spatial coverage and magnitude in February-early March (Figures 4a and 4b), and weak in the months May-September, with the smallest spatial coverage and magnitude in May (Figures 4c and 4d). In the southern NBC-box (6°N–10°N, 51°W–59°W), BLT peaks in June-July (Figures 4e and 4f) decreasing toward October. During winter and spring BLT in the southern NBC-box is still large, but more sporadic.

The seasonal cycle of the area-averaged BLT for the southern NBC-box (Figure 5a) shows that BLT peaks in the model in the summer months of June/July, with a tendency for an overestimation when using monthly profiles instead of daily. The EN4 analysis, in contrast, shows a maximum in March decreasing toward September, completely missing the simulated summer peak BLT. The DeBoyer climatology shows an overall constant value throughout winter and spring. The EN4 profiles, on the other hand, corroborate the

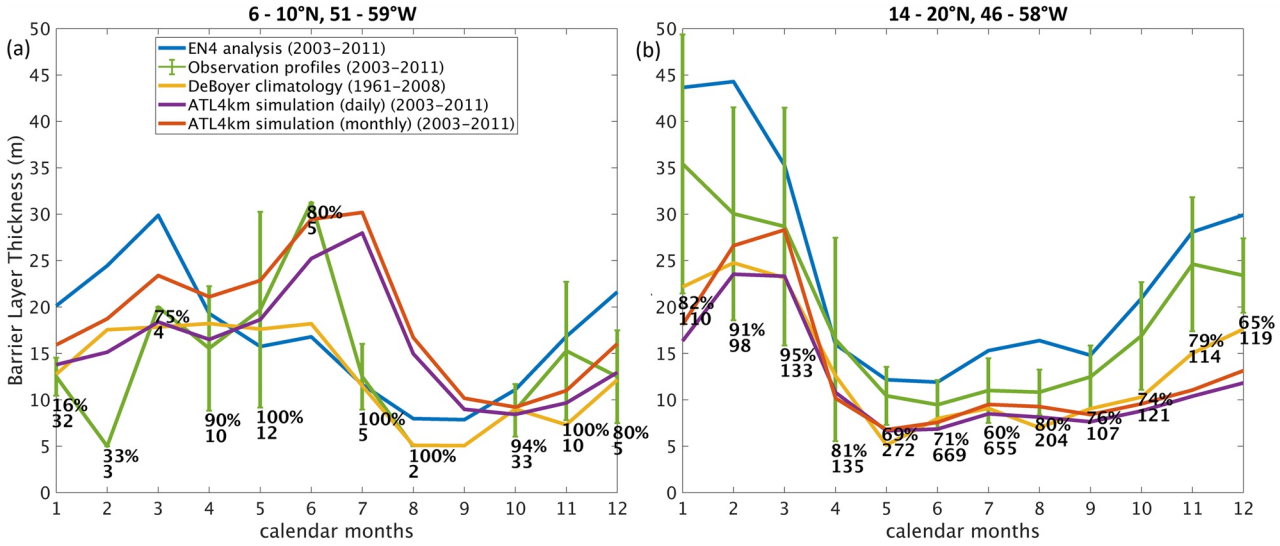

Figure 5. Monthly variability of area-averaged BLT (meters) in the (a) NBC region (6°N–10°N, 51°W–59°W) and (b) NEC region (14°N–20°N, 46°W–58°W), from EN4 objective analyzed data (2003–2011, blue), Observation profiles (2003–2011, green), DeBoyer climatology (1961–2008, yellow), ATL4km simulation with daily data (2003–2011, violet) and with monthly data (2003–2011, red). The values at the bottom of the error bars represent the percentage of the number of profiles with barrier layers (top number) with respect to the total number of profiles present (bottom number) for that month in the period 2003–2011. BLT, barrier layer thickness; NBC, North Brazil Current; NEC, North Equatorial Current.

existence of a maximum in June (being seen in 80% of the profiles). There are, however, only 5 profiles in this region in June (and in general not many over the whole year), making the observational estimates rather uncertain.

For this box, the seasonality and spatial distribution of BLT in the model and observations (Figures 3–5) found in our work also agrees with the findings of Pailler et al. (1999) and Masson and Delecluse (2001) for the region south of 10°N, where the NBC rings and the Amazon and Orinoco river plumes are at their peak in summer.

The seasonal cycle of area-average BLT in the northern NEC region (14°N–20°N, 46°W–58°W) from the ATL4km, DeBoyer climatology, and EN4 analysis and profiles is presented in Figure 5b. In this NEC-box, there is a good agreement between all data sets in terms of temporal evolution. As was seen in the spatial comparisons, the temporal plot also shows largest BLT occurring during winter months of December-March, when the EN4 analysis and profiles show larger values compared to the rest of the data sets, which in turn peak in February-March. A seasonal minimum is seen in May. The ATL4km simulation agrees well with the DeBoyer climatology but seems to underestimate the EN4 estimates. This can be partly due to the above discussed tendency to lower the estimates when complete coverage in space and time is taken into account.

In summary, BLT daily fields from ATL4km for the period 2003–2011 showed two distinct localized regions with barrier layers having different seasonal cycles: 1) thick barrier layers in the NBC area in June-August, and 2) thick barrier layers in the NEC region during January-March. An explanation for this seasonality of BLT is given in the following sections with details on the mechanisms responsible for the growth and decay of the barrier layers at those two locations.

4. Barrier Layer Growth and Decay in the NBC Rings Area

The regional circulation in the western tropical Atlantic is dominated by the NBC, an intense western boundary current. The maximum Amazon discharge during May-June (Fournier et al., 2017; Masson & Delecluse, 2001; Silva et al., 2005; Varona et al., 2019), and Orinoco discharge during July-August (Fournier et al., 2017) causes a surface plume of freshwater which spreads northwestward due to the NBC and associated rings, not just during the months of maximum river discharge, but all year round. Previous studies have shed some light on the advection of the Amazon/Orinoco freshwater and their interaction with the

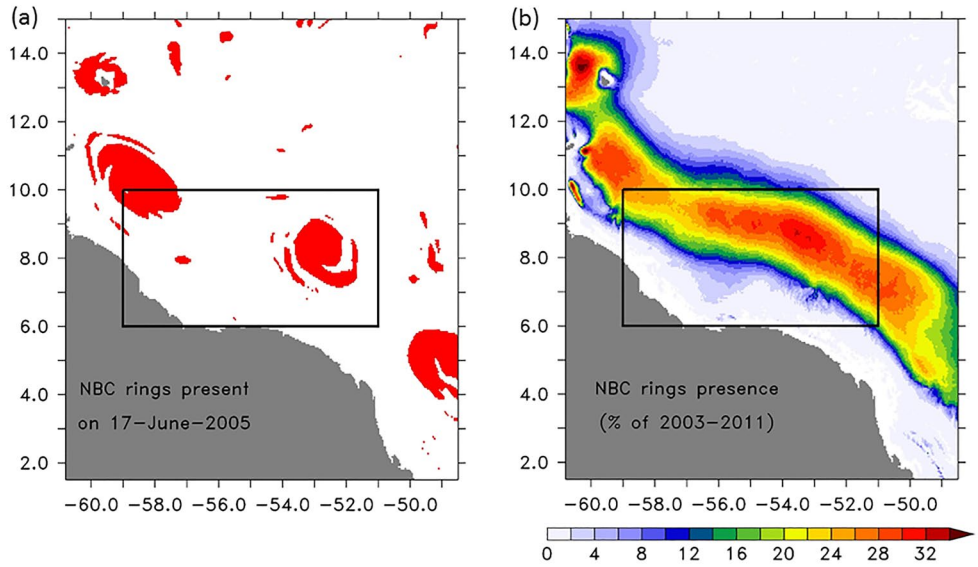

Figure 6. (a) Simulated NBC rings shown as an instantaneous mask, defined using a criteria which uses the Okubo-Weiss parameter and relative vorticity. (b) Percentage of the nine years (2003–2011) when NBC rings are present. The black box encloses the studied NBC rings region (6°N–10°N, 51°W–59°W NBC-box). NBC, North Brazil Current.

seasonally varying NBC and NBC rings (Ffield, 2007; Fournier et al., 2017; Fratantoni & Glickson, 2002). This interplay between river runoff and surface ocean dynamics cause the emergence of variability in barrier layer formation associated with the NBC rings, which is the topic explored in this section. To our knowledge, the relation between BLT and NBC rings has never been studied in detail, though barrier layers have been observed in a Caribbean Sea eddy in September 2014, suspected to originate from the NBC (Rudzin et al., 2017) and in another eddy in February 2018 also in the Caribbean Sea (van der Boog et al., 2019). In the latter case, the surface water in the eddy is suggested to originate from the Orinoco River.

Through inspection of daily fields of the zero line of meridional velocity at every model depth level, the east and west limits of the NBC were determined, with the NBC seen to extend down to about 150 m depth, beyond which depth the current becomes very faint and the North Brazil Undercurrent (NBUC) emerges. Daily fields of temperature and salinity in the NBC show that the NBC carries cool (17°C–25°C) and saline (>36 psu) water from 5°S to around 6°N and northwards at depths 50–180 m. Warmer (>26°C) and fresher (34–35.5 psu) water is transported by this current starting from the Amazon mouth at 0°N50°W toward the northwest, at depths from surface down to 50–80 m. The time series of meridional non-recirculated freshwater transport by the NBC (not shown) reveals how much of this freshwater discharged from the Amazon and Orinoco rivers is transported northward. The simulation for years 2003–2011 shows a high seasonality in the NBC transports. The freshwater transport signals start from the equator and propagate to 10°N in a span of 2–3 months, with a maximum transport being in the months of May-August, peaking in July. The non-recirculated transport for July 2007 is 24.45 Sv at 2.3°N. According to Hellweger and Gordon (2002), the Amazon plume water takes around 2–3 months to reach the Barbados Island at 13°N, after the maximum Amazon discharge in May. Our results corroborate this observation. The Amazon discharge is the lowest from October to February (Fournier et al., 2017; Masson & Delecluse, 2001; Silva et al., 2005; Varona et al., 2019), also seen in the individual daily SSS model fields.

The simulated NBC rings were tracked using daily fields of the Okubo-Weiss parameter and of relative vorticity, according to a criterion involving negative values of the Okubo-Weiss parameter and positive values of relative vorticity. It was seen that an average of six large NBC rings plus a few smaller rings in a total of 7–9 eddies form every year in the model in the period 2003–2011, a total of 75 rings in the 9 simulated years. An instantaneous view of the existing rings on the June 17, 2005 is presented in Figure 6a, which shows a mask defining the eddies, computed based on the criterion described above. North of 5°N the NBC breaks down into NBC rings, mainly forming around 6°N–9°N. NBC rings have been characterized earlier with

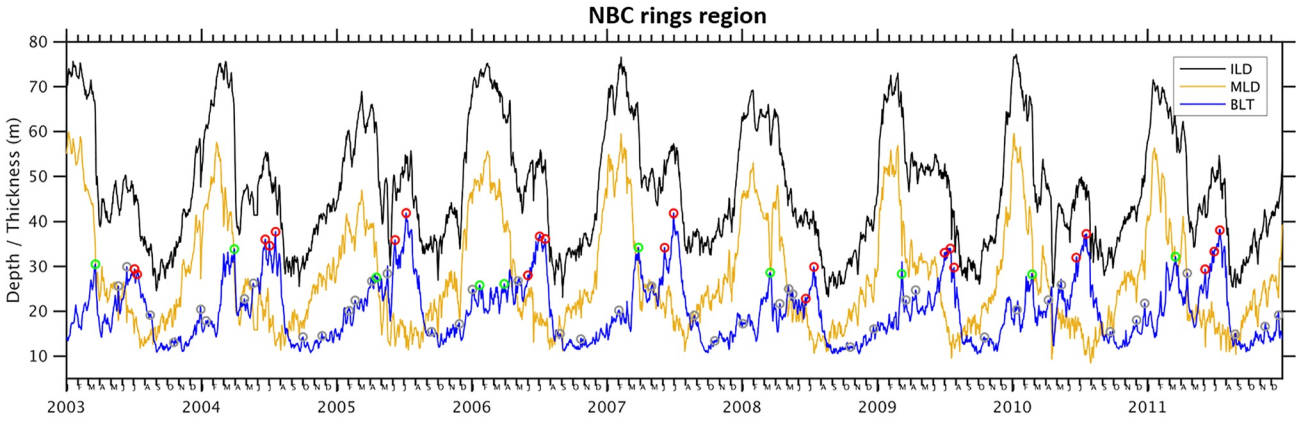

Figure 7. Daily time series of area-averaged ILD (black), MLD (gray) and BLT (blue) (meters) in the region of NBC rings (NBC-box, 6°N–10°N, 51°W–59°W). Red circles are events of large BLT in summer. Green circles are events of large BLT in winter. BLT, barrier layer thickness; ILD, isothermal layer depth; MLD, mixed layer depth; NBC, North Brazil Current.

observations (Fratantoni & Glickson, 2002; Fratantoni & Richardson, 2006; Schiller & Smith, 2018) and simulations (Jochum & Malanotte-Rizzoli, 2003). They have a diameter ranging from 100 to 500 km and form throughout the year. Most of the rings last for 3–5 months and travel along a "corridor" offshore the south American coast, reaching up to 13°N–15°N, with some surviving up to 18°N (Figure 6). In the simulated 9 years, the studied southern box encloses the region where the passage of NBC rings is more frequent, as can be seen by the "heat" map in Figure 6b.

Daily area-averaged ILD, MLD, and BLT for the southern NBC-box (6°N–10°N, 51°W–59°W) are shown in Figure 7. Large BLT is found from May to August, thickest being in late June-July (blue curve in Figure 7). All the events enclosed in circles are cases when there are barrier layers present in the NBC rings. The green circles depict rings formed in winter or spring, when the NBC retroflection is further to the northwest, and the red circles correspond to rings generated in summer, when the retroflection into the NECC is more pronounced. A total of 22 NBC rings had the thickest barrier layers in summer and 10 NBC rings had large BLT in late winter-spring.

Our investigation of the mechanisms behind the growth and decay of barrier layers in this NBC region will be conducted separately for the seasonal cycle and for the extreme isolated events, since they have different reasons. Before we take a look at those events marked with circles in Figure 7, we will first focus on the seasonal evolution over which the events are superimposed.

4.1. Mechanisms Behind the Seasonal Evolution

Figure 7 shows that the ILD and MLD are deep every winter. This is due to the well-known winter convective mixing in the upper ocean, when the cool, saline and dense water on the surface sinks and when there is mixing in the upper layer due to intense wind stirring caused by strong trade winds, as shown by Foltz et al. (2004) and Foltz and McPhaden (2008).

Typical in summer are shallow mixed and isothermal layers due to higher surface temperatures than in winter. The MLD is shallow in summer also because of the large freshwater outflow from the rivers in May-July and the large transport and spreading of this freshwater by the NBC and its rings in July. The MLD remains shallow until October, as the surface water still remains fresher due to the river plume water, and starts increasing only after November. But the deepening of the isothermal layer from May to August in spite of the warm water at the surface is a peculiarity seen in Figure 7. A deep ILD and a shallow MLD are both responsible for the BLT being large during that period of the year, but to a certain extent the magnitude of BLT is determined by the deepening of ILD from May to August. In winter, the BLT is small in this southern box, having only a few peaks every year (total 10 peaks encircled in green in Figure 7).

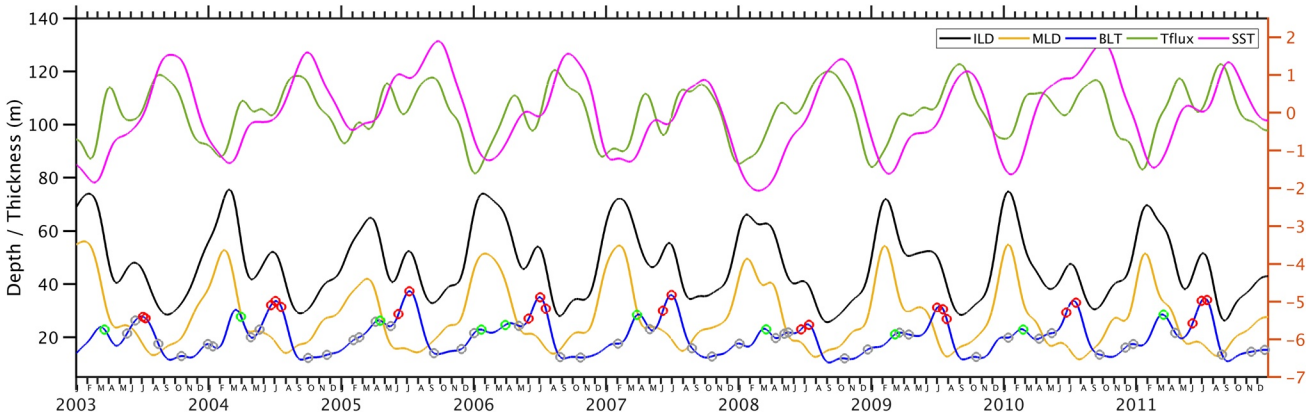

Figure 8. Time series of ILD, MLD, and BLT, normalized net surface heat flux and normalized SST low-pass filtered with a 60 days cut-off filter. Red circles depict events when the eddies have large summer BLT; green circles show events when the eddies have large winter BLT; gray circles correspond to the remaining eddies which have significant BLT. BLT, barrier layer thickness; ILD, isothermal layer depth; MLD, mixed layer depth; SST, sea surface temperature; NBC, North Brazil Current.

Since this box is populated by NBC rings, the first question to answer is if the seasonal behavior in the box is imposed by what is happening in the core of the rings, or if, on the other hand, the rings are acquiring the seasonal evolution of ILD and MLD from their periphery, that is, from the large scale seasonal evolution of temperature and salinity. To that end, the eddies were tracked as mentioned and those quantities (ILD, MLD, and BLT) where masked, therefore isolating what is happening in the core of the eddies. Averaging over only the cores of the NBC rings, the same behavior as in Figure 7 was seen (not shown).

Most of the times a barrier layer is created near the Amazon/Orinoco shelf break due to the tilting of the strong salinity fronts created at the plume edge, as the freshwater immediately comes in contact with the saline ocean water (Silva et al., 2005). Daily distributions of BLT from 2003 to 2011 in the ATL4km simulation show that the NBC rings transport the conditions for barrier layer maintenance, which were formed near the Amazon/Orinoco shelf break. But the barrier layers can also newly form within NBC rings themselves when the ring starts to generate, as we will see next. The barrier layers in the NBC rings erode away as the ring dissipates, sometimes in the Caribbean Sea, and sometimes in the east of the Lesser Antilles after interacting with the chain of islands.

There is a positive linear relation between MLD and ILD within the cores of NBC rings generated throughout the year except in June and July (marked with red circles in Figure 7). This is because during those months there is an increase in ILD inside the eddy (also seen in Figure 7, reason to be seen ahead), while the MLD remains nearly constant.

In order to check if the seasonal evolution in ILD, MLD, and BLT between the core of the NBC rings and their periphery differs, a climatology of the area average of these quantities over the core and only over the periphery were computed separately. Again no significant difference in the seasonal evolution was seen, meaning that the core of the eddies mainly acquires the seasonal conditions for the development of the barrier layers from the background where they are embedded. Furthermore, two regions following the eddy translation were analyzed, one more to the east, closer to the generation region and one in the west, where the eddies are matured and dissipate. The eddy cores in the east have the deepest winter MLD and ILD in February, however the BLT curve in March is much smaller than that further downstream in the west. In May-June the MLD remains almost constant and the ILD increases, causing a second pronounced peak BLT in July. In the west, instead, the late winter peak is larger or comparable to the summer one. This reveals that the eddies experience different conditions as they travel downstream to the northwest. The difference seem to be attributable to the March MLD, which in the west decreases faster than in the east.

In order to more easily correlate the ILD, MLD, and BLT seasonal evolution in the NBC-box with surface fields of temperature and of atmospheric forcing, the time series in Figure 7 were low-pass filtered with a cut-off period of 60 days (Figure 8). As can be immediately seen, the summer maximum of BLT is always

associated to a second deepening of the ILD in June/July, with the MLD shoaling progressively toward the peak of summer.

The reasons behind this behavior are various. On one hand, there is freshwater carried in the periphery of the NBC rings, what causes mostly the MLD to shoal due to salinity stratification being strong. On the other hand, and more importantly, during the second maximum in ILD magnitude, one can observe a plateau in the warming trend toward summer, as seen in the SST seasonal evolution. This small plateau (or even in some years an actual reduction in SST) is associated to a pronounced reduction in the net heat flux forcing the upper ocean. So, the semi-annual cycle in net heat fluxes in the region imparts a tendency for a reduction in the warming in June-July of the surface and subsurface. As a consequence, the layers below the surface remain more homogeneous (and sometimes develop a temperature inversion, when the surface is colder than the subsurface) and the ILD criterion (SST − 0.2°C) is met at deeper depths. If the heat fluxes would only show an increase toward summer, the continuous warming of the surface and subsurface would lead to a fast development of a strong seasonal thermocline, resulting in a small ILD, which together with an also small MLD would lead to a vanishing barrier layer. That is seen to happen during September. In conclusion, in this region of NBC rings, the seasonal BLT time series match that of the seasonal ILD more than that of the seasonal MLD. The reason seems to be the behavior of the net heat fluxes, which show a relative minimum during late spring-early summer.

When removing the low-pass filtered version of ILD, MLD, and BLT from the original time series, the remaining high-frequency variations have an overall amplitude of about 10 m with strong amplitude events occurring in spring reaching 15 m (not shown). Nearly all events correspond to the time when a NBC ring was present in the box. It is therefore concluded that, in the region, the passage/presence of eddies is responsible for the emergence of large amplitude BLT variations. In the following section we will focus on those events and search for the mechanisms responsible for the large BLT associated with NBC rings.

4.2. Mechanisms Behind Short Timescale Events

In the following, we present results regarding the analysis of the summer cases of high-frequency barrier layer growth/decay in NBC rings (22 cases).

4.2.1. Barrier Layer Growth

In the NBC rings area, the evolution of the summer BLT, the period of seasonally large barrier layers, is caused mainly by changes in ILD. Figure 9 shows a snapshot of BLT and variables affecting it for a day with large BLT in one of the NBC rings (this episode corresponds to one of the red circles in Figure 7).

The largest BLT in the box (about 85 m) is concentrated in the anticyclonic eddy, depicted by the clockwise pattern of currents. As most of the NBC rings, this ring forms around 6°N from the NBC retroflection and transports to the northwest at its periphery fresh Amazon water after its maximum discharge in May-June. The NBC ring itself encloses a mass of comparatively higher salinity water inside its core (SSS around 34 psu) than at the periphery (SSS around 33 psu) (Figure 9d), with the large BLT not coinciding with the locations of fresher surface water. The ILD, with a maximum at the core of the eddy of about 95 m, causes the BLT to be maximum at the eddy core (Figure 9b). The MLD in the ring, in turn, is small and does not have as high a difference from its surrounding as in the case of ILD.

As discussed earlier, the NBC transport is maximum in June-August and the magnitude of the top 150 m transport is large at the NBC in Figure 9e on this day, transporting the fresher water from the river mouth to the northwest. Moreover, the ITCZ is at its northernmost location at this time of year, shown by Foltz et al. (2004) and Foltz and McPhaden (2008) (their Figure 1). The E-P-R is therefore negative up to 15°N in these months on the region of low SSS (Figures 9h and 9d). SST is high in regions of large BLT, as summer conditions prevail during the shown snapshot. In summer, the SST is larger in the Atlantic Warm Pool (Liu et al., 2012) encompassing this region. All in all, from Figure 9, the spatial distribution of barrier layers resemble the spatial distribution of SSS and surface currents. However, the localization of the maximum BLT in the core of the NBC eddy is unexpected and will be studied in detail next.

In order to study the mechanisms that are responsible for the growth of the barrier layers, the terms of the temperature and salinity vertical gradient balance equations (Equations 3 and 4 in Section 2) were

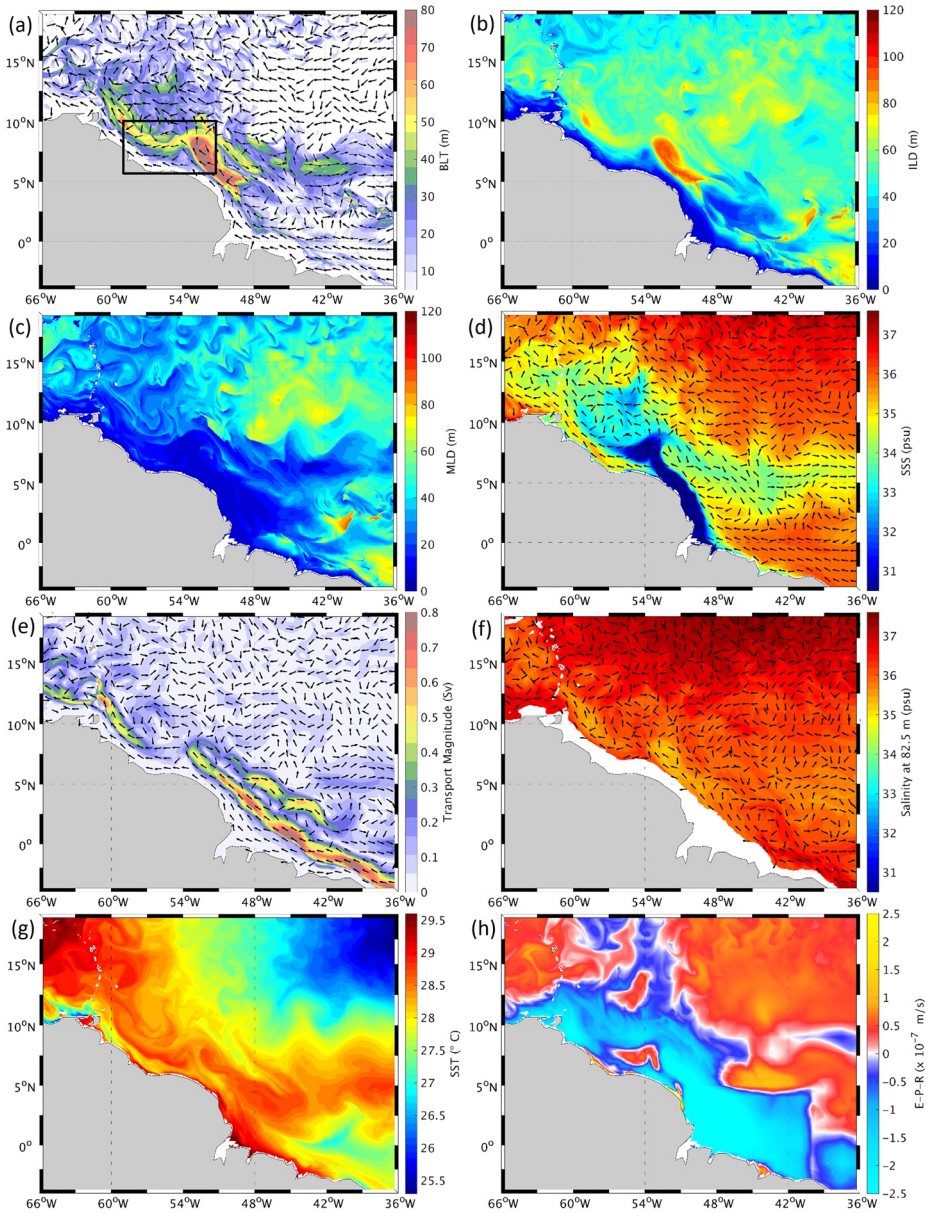

Figure 9. Snapshots for June 30, 2007 (summer) of (a) BLT (meters) with vectors showing surface currents, (b) ILD (meters), (c) MLD (meters), (d) SSS (psu) with vectors showing surface currents, (e) top 152.5 m horizontal transport magnitude (Sv) and direction, (f) salinity (psu) at 82.5 m with corresponding currents, (g) SST (°C) and (h) E-P-R ($\times 10^{-7}$ m/s). BLT, barrier layer thickness; ILD, isothermal layer depth; MLD, mixed layer depth; SSS, sea surface salinity; SST, sea surface temperature.

computed on a daily basis and averaged over the day of the event of maximum BLT in the ring (June 30, 2007) and 2 days before this date (i.e., a 3-days average). With this, we can study the behavior of the physical mechanisms (each of the terms in the balance) acting between two days before the event and the event day, when the resulting ILD, MLD, and BLT are seen (Figure 10). With the balance terms we are able to quantify the contribution of each term in bringing about the change in ILD and MLD needed to explain the observed BLT distribution. Since the focus is to explain the high-frequency event, the averaging period is small.

We focus on the changes at a section across which the NBC ring passes. This section is taken at 52.32°W (from 5.5°N to 10°N) through the core of the NBC ring seen on June 30, 2007 (Figure 10). From this figure (see dashed and solid lines) it is clear that, from the June 28, 2007 to the June 30, 2007, what changed was

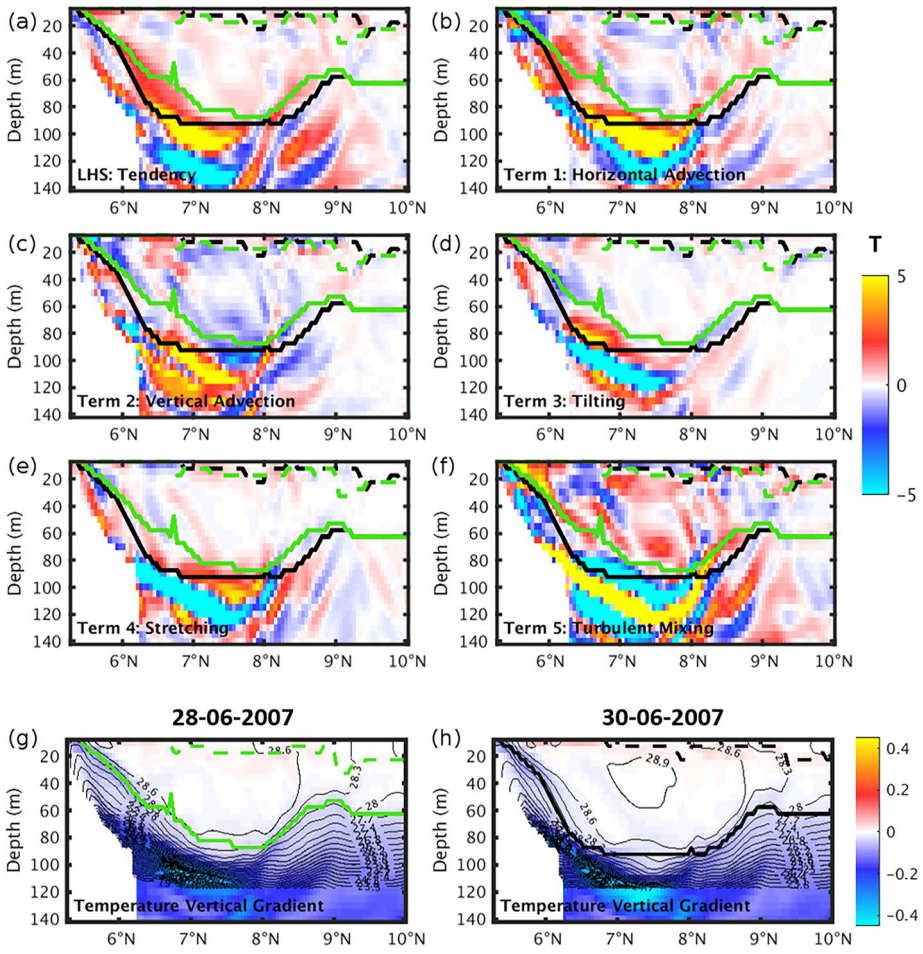

Figure 10. Vertical section at 52.32°W through the core of the NBC ring present on June 30, 2007 in the southern NBC-box. Temperature gradient balance terms (a) LHS; (b) Term 1: Horizontal advection; (c) Term 2: Vertical advection; (d) Term 3: Tilting; (e) Term 4: Stretching; (f) Term 5: Turbulent mixing, averaged from June 28, 2007 to June 30, 2007, units ($\times 10^{-7}$°C/m.s). Temperature vertical gradient (°C/m) with contours being isotherms (°C) are shown for (g) June 28, 2007 and (h) June 30, 2007. Black (green) solid line correspond to the ILD, black (green) dashed line corresponds to the MLD for June 30, 2007 (June 28, 2007).

a deepening of the ILD, as seen by the change in position of the solid green to solid black curves. When looking at the tendency term (Figure 10a), it is clear that co-located with this change there is a positive temperature gradient tendency from the June 28, 2007 to the June 30, 2007 at those particular depths. We note that stronger changes are seen elsewhere outside the barrier layer, namely in the eddy peripheries, where strong dynamical or thermodynamic changes occur. They are not of relevance for explaining the signal at hand, which lies in between the green and black curves.

From Figures 10g and 10h we see that the temperature gradient drastically increased in the southern part of the ring in the region where the ILD resides during June 30, 2007. Furthermore, we see a moving apart of the isotherms on the southern lateral edge and a downward shift of the isotherms in the region between the green and black curves from June 28, 2007 to the June 30, 2007. This corroborates the computed positive temperature gradient tendency seen in the tendency term. Looking now at the terms in the RHS of the balance equations (Figures 10b–10f), the summation of which give the left hand side (LHS) term, one sees a large amount of compensation in the patterns. In the region between the green and black curves, the dominant mechanisms causing the isotherms to move apart on the south and shift downward in general, in the process growing the ILD, are horizontal advection and to a minor extent vertical advection, tilting and

stretching (Figures 10b–10e). Turbulent mixing (Figure 10f) balances only partly the above terms, so that a residual positive tendency results.

In the presented event, at the lateral edges of the barrier layer, the processes acting are mainly horizontal advection (depths of 40–80 m), stretching and tilting. At the bottom of the barrier layer, horizontal advection and stretching sum up, with mixing partially canceling them. The salinity vertical gradient balance equation terms are not discussed in this case since 1) we see negligible changes in MLD and 2) the ILD is solely dependent on temperature.

From an inspection of every summer event showing a peak in the BLT time series (all red circles in Figure 7), it was inferred that when the ILD grows, the temperature vertical gradient tendency between the days before and the resulting ILD is mostly positive. From all analyzed summer events, the ILD grows 1) when the isotherms move apart (16/22 cases) or 2) when the isotherms move together but the gradient deepens (6/22 cases).

4.2.2. Barrier Layer Decay

To investigate the mechanisms responsible for the decay of the high-frequency barrier layer events in NBC rings, we averaged the terms over a period of three days from the day when the BLT is at its peak to the day when an afterward significant change in ILD/MLD is seen, that is, when an increase in MLD and/or a decrease in ILD occurs in the NBC ring.

The barrier layers in NBC rings get usually thinner when the ILD gets smaller. After examining the decay of the barrier layers in all the 22 events it was observed that the temperature vertical gradient tendency is mostly negative. Associated to the reduction in ILD, in most cases (17/22 cases, 77.3%) the isotherms are moving vertically apart. One of these decay events is shown in Figure 11, occurring from July 11, 2003 to July 13, 2003. The vertical section is now taken at 56.12°W through the core of the eddy on July 11, 2003 and the change in BLT two days after is studied.

From the temperature vertical gradients with isotherms superimposed in Figures 11g and 11h, it is noticeable that the ILD shoaled, as the isotherms around the ILD moved vertically apart. In the tendency term (LHS) in Figure 11a one sees a negative tendency between the solid black and solid green curves, which led to the ILD criterion being met at a shallower depth. The dominating term contributing to the negative temperature gradient tendency is again horizontal advection in the southern part of the eddy and stretching in the base of the isothermal layer (Figure 11e). Turbulent mixing once again opposes the horizontal advection to the south but contributes slightly to the LHS tendency at the isothermal layer base, as seen in Figures 11b and 11f. In this event there is negligible change in MLD compared to ILD.

The decay of the barrier layer happens also due to the deepening of the mixed layer in certain cases. The deepening of the mixed layer is associated with a negative salinity vertical gradient tendency, which indicates a reduction in salinity vertical gradient between the MLD of the day of peak BLT in the ring and 2 days after. It occurs due to the stretching of isohalines, with in this case horizontal advection, stretching and tilting being dominant for deepening the MLD.

In conclusion, we saw in this section that the BLT is at its maximum in the region of NBC rings during the summer months of June-August and has a seasonal minimum in fall. The high-frequency, event-like growth of the ILD and consequent growth of the barrier layer is associated with a stretching of isotherms most of the times. Horizontal advection, tilting and stretching are dominant processes in generating a barrier layer in the NBC rings. ILD shoals and reduces the barrier layer again by stretching of isotherms. The evolution of barrier layers here is controlled more by the changes in ILD than in MLD.

In winter there are fewer rings with barrier layers in them (green circles in Figure 7). NBC rings in winter have larger BLT in their periphery, rather than in the core. The shoaling of the MLD by horizontal advection and turbulent mixing of freshwater in the periphery of the NBC rings and a tilting of the salinity fronts is rather responsible for growing those barrier layers, than an increase in ILD. But in the decay phase, an increase of MLD and a decrease of ILD both are equally responsible.

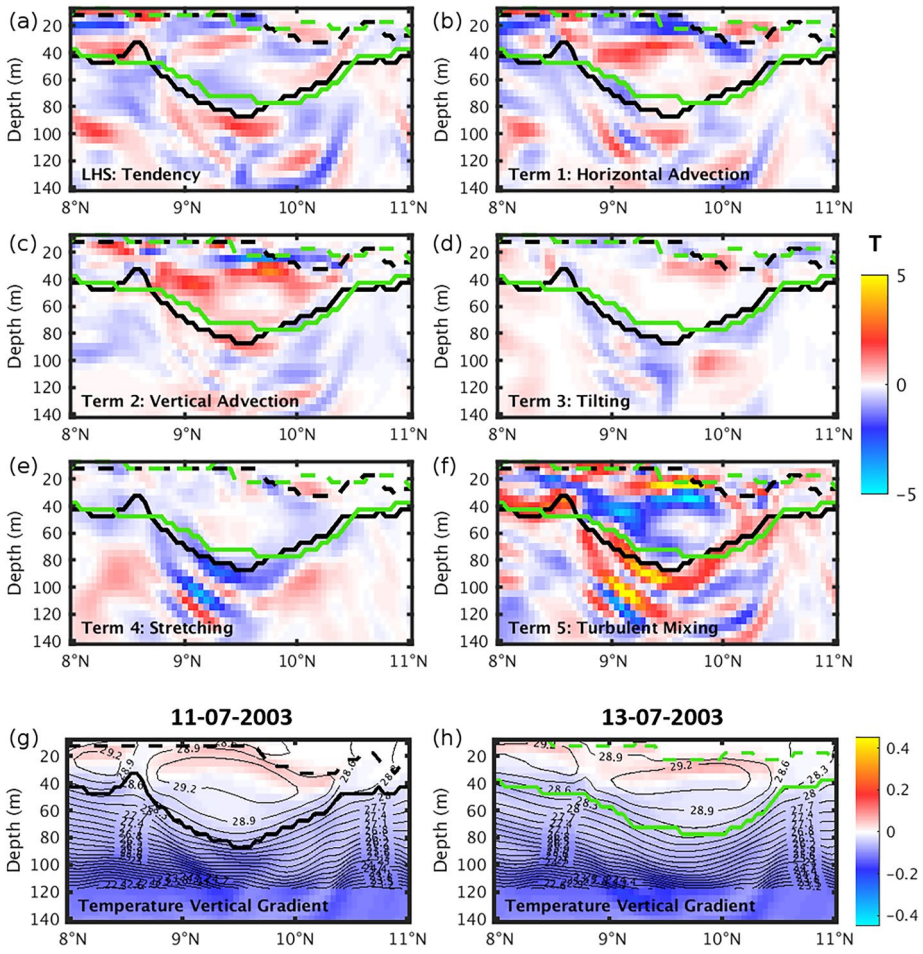

Figure 11. Same as Figure 10, but for a vertical section at 56.12°W through the core of the NBC ring present on July 11, 2003. Balance terms are averaged from July 11, 2003 to July 13, 2003. Black (green) solid lines correspond to the ILD, black (green) dashed lines to the MLD for July 11, 2003 (July 13, 2003).

5. Barrier Layer Growth and Decay in the NEC Region

The NEC area studied here resides in the southern part of the subtropical gyre, where barrier layers persist almost throughout the year. Figure 12 shows the simulated daily variability of ILD, MLD, and BLT for 2003–2011 in the NEC-box. During December-March there are thick barrier layers, with the largest extent being in February-March. From April-May onwards, the BLT has small amplitudes, increasing slightly in July-August, and thinning again in September-November (Figures 5b and 12). As for the NBC area, besides the dominant seasonal signal in BLT, there is high-frequency variability superimposed, although of much smaller amplitude than in the previous section. Those short events are marked in red circles (29 events) and in green circles (7 events), the latter corresponding to events after which the winter BLT is completely eroded. The growth and decay of the seasonal barrier layer and of the individual peak events were investigated and results are presented next.

5.1. Mechanisms Behind the Seasonal Evolution

The ILD and MLD have similar seasonality, being large in winter due to wind- and buoyancy-induced mixing and presenting a secondary maximum in May-July. The MLD in winter overlies, however, a relatively deep isothermal layer, giving rise to the large barrier layers in winter (Figure 12, blue curve). During the secondary maximum, ILD and MLD roughly have the same behavior, leading to reduced or almost vanishing barrier layers.

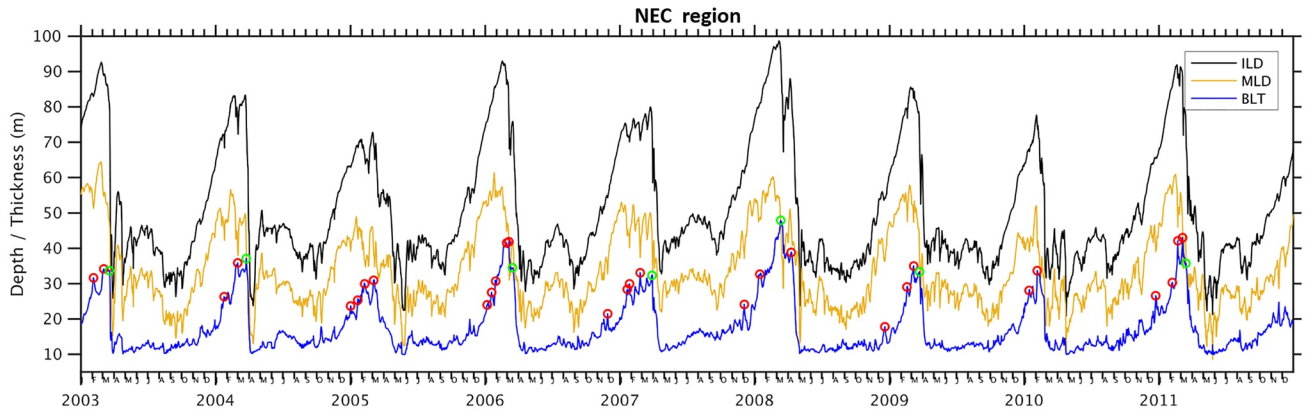

Figure 12. Daily time series of area-averaged ILD (black), MLD (yellow) and BLT (blue) (meters) in the NEC region (14°N–20°N, 46°W–58°W). Red circles denote the large peak events of BLT. Green circles indicate the events when the winter barrier layer peaks before getting eroded in spring. BLT, barrier layer thickness; ILD, isothermal layer depth; MLD, mixed layer depth; NEC, North Equatorial Current.

As seen so far in Figures 3, 5b, and 12, the maximum seasonal BLT is in winter. Figure 13 presents a vertical section at 53.72°W (between 15°N and 20°N) of the salinity and temperature gradient balance terms. They are averaged from November to February in order to retain the main contribution at the seasonal scale (with the contribution from all small scale events being averaged out). The black and green curves in the figure show how the MLD and ILD change from November, when the barrier layer just starts to form, to February, when there is a maximum BLT.

The BLT growth from November to February is due to a large ILD growth and a comparatively small MLD growth (as depicted, respectively, by the solid, and dashed lines in Figure 13). The isothermal layer deepens because of turbulent mixing, as this term contributes most to the positive temperature vertical gradient tendency between the ILD in November and February (Figures 13b and 13l). In our opinion, this is due to winter convective mixing due to cooling or wind forcing. On the other hand, the salinity gradient tendency shows only small values between the mixed layers in November and February. In fact, the strong turbulent mixing in the salinity case is balanced by the tilting of the salinity field (Figures 13g and 13k) and the resultant small signal in the tendency mostly is a consequence of horizontal/vertical advection (Figures 13c and 13e).

There is a somehow abrupt seasonal decay of the barrier layers from March to April. We see that the barrier layers are destroyed due to a shallowing of the ILD and MLD, that is the opposite situation compared to the slow growth during fall and winter. The negative temperature vertical gradient tendency between the ILD in March and April is again due to a contribution of turbulent mixing of the warmer water on top in spring, which destroys the barrier layer during that season. The MLD reduces due to tilting and stretching and moderately due to turbulent mixing (not shown).

After the erosion of the winter BLT in spring, a comparatively thinner BLT grows from May to July and decays in September (Figure 12). In summer, compared to winter, increased surface heating stratifies the surface layer, reducing the ILD. As in the NBC area, a semi-annual behavior of net heat flux, SST and wind stress magnitude exists in this region. There is a reduction in SST due to the forcing from the reduction in net heat flux and a second peak in wind stress magnitude in July. Convective and wind mixing therefore cause the small increase in ILD and MLD. Turbulent mixing of temperature mainly contributed to the positive temperature gradient between the ILDs in May and July (not shown). Additionally, during summer the maximum spatial extent of spread of the freshwater from the Amazon and Orinoco rivers occurs and the ITCZ reaches its northernmost position. The seasonal maximum transport of NBC in July, carrying the above fresher water northwards, and the seasonal maximum NEC in late-summer getting salty water from the open ocean to the west, cause tilting of salinity fronts and shoal the MLD. The shoaling MLD over the slightly deepened ILD gives rise to this thin summer BLT. Alternatively, the increase in ILD due to penetrating solar radiation, with MLD maintained at constant depth in summer, could also cause this thin barrier

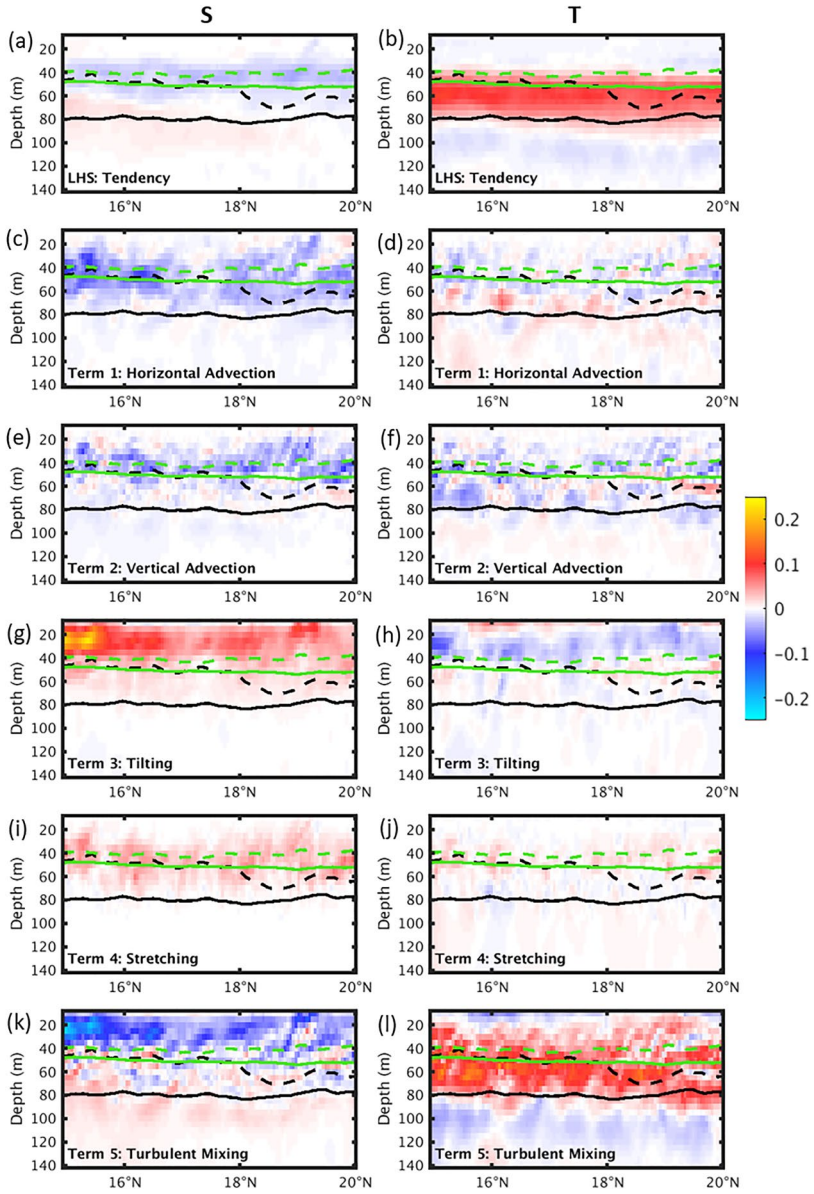

Figure 13. Vertical section at 53.72°W through the maximum climatological BLT in February of salinity and temperature gradient balance terms: (a), (b) LHS; (c), (d) Term 1: Horizontal advection; (e), (f) Term 2: Vertical advection; (g), (h) Term 3: Tilting; (i), (j) Term 4: Stretching; (k), (l) Term 5: Turbulent mixing (units are $\times 10^{-7}$ psu/m.s and $\times 10^{-7}$°C/m.s, respectively). Terms are averaged from November to February. Black (green) solid line is ILD, black (green) dashed line is MLD for February (November). BLT, barrier layer thickness; ILD, isothermal layer depth; MLD, mixed layer depth; LHS, left hand side.

layer to occur (Mignot et al., 2012). Turbulent mixing and tilting shoal the ILD from July to September, causing the thin summer BLT to decay.

5.2. Mechanisms Behind Short Timescale Events

5.2.1. Barrier Layer Growth

By closely inspecting the daily evolution in the simulation, it was seen that during September-November, horizontal advection of the existing runoff and precipitation freshwater takes place up to 23°N. As seen in the seasonal evolution, the ILD and MLD start both to become deep in late fall, but with the MLD change,

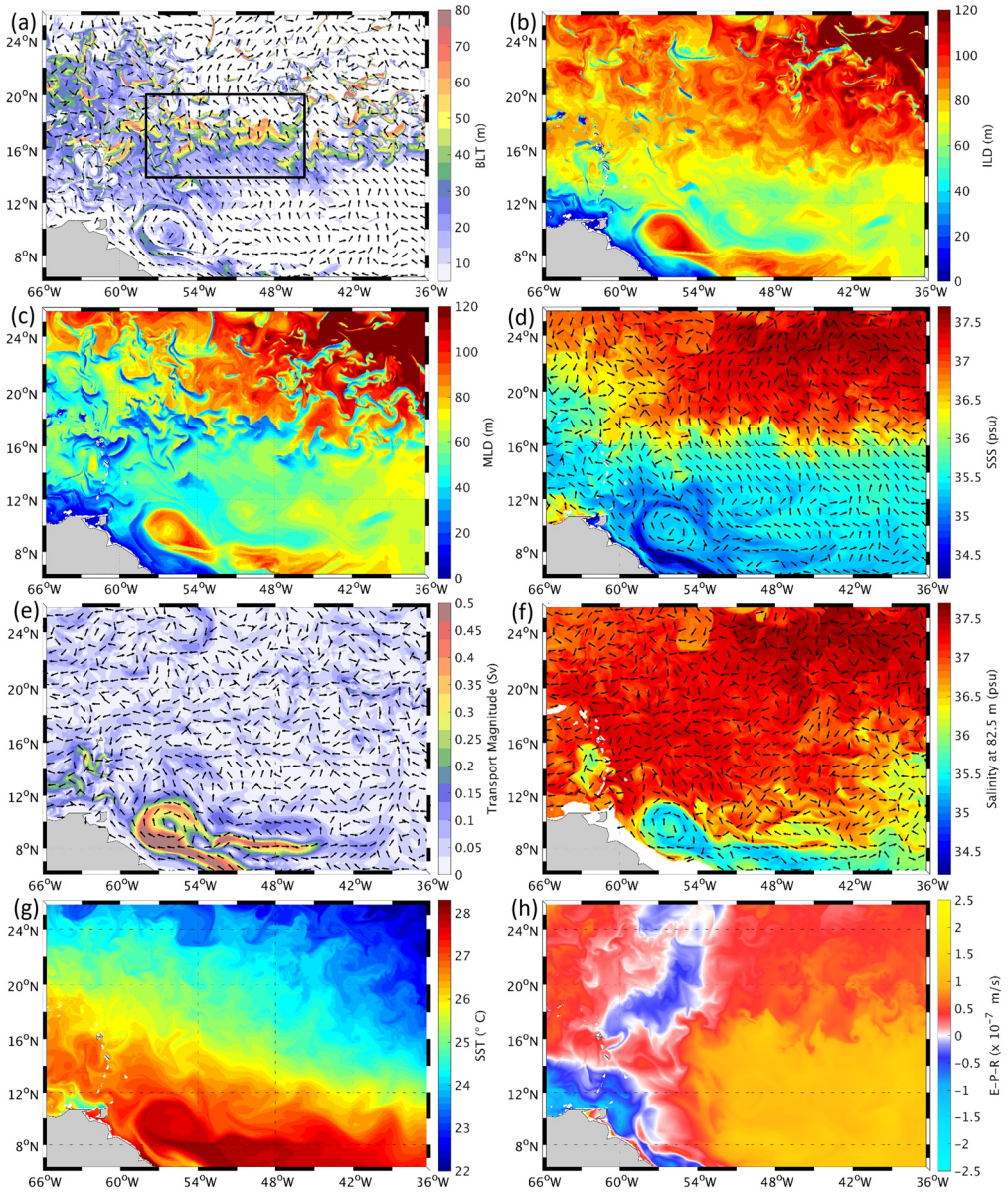

Figure 14. Same as Figure 9, but for a winter event of barrier layers in the NEC region in February 17, 2009. NEC, North Equatorial Current.

in comparison to ILD, staying small. In October-January, the formation of barrier layers at the fresher side of the large-scale salinity front occurs in the form of faint filaments. The resulting BLT becomes maximum in February-March at 15°N–18°N. We now focus on those small-scale and highly frequent events superimposed on the seasonal evolution.

Figure 14a presents the BLT from one of the peak events (red circles in Figure 12) in February 17, 2009. The figure shows the BLT distribution in the middle of the winter season, when it is growing to reach its maximum extent. It can be seen that barrier layers occur on the lower SSS side of the large-scale salinity front (compare Figures 14a and 14d). From December to February, E-P-R is strongly positive from 5°N northwards (Figure 14h), meaning more evaporation in the place of this barrier layer than freshwater flux by precipitation. In fact, during this time of year, the ITCZ is located south of this region, and there are dominant easterly trade winds (Foltz et al. (2004) and Figure 1 of Foltz and McPhaden (2008)), which cause the large evaporation in this region. From November to March around 15°N, the salinity in the upper ocean is

higher (Figure 14d) and water is colder (Figure 14g) as compared to summer (Figures 9d and 9g). Therefore, the cool, saline, dense surface water sinks in convective mixing processes. This, along with the wind stirring, causes the larger ILD and MLD in winter than in summer.

BLT of up to 40–80 m is present from 13°N to 22°N, with a maximum being located at 15°N–18°N. Those barrier layers align in an interesting pattern of very localized variability, in general terms, confined to the salinity frontal region. The ILD is deep (90–120 m) in this region and time of year (Figure 14b). The MLD is shallow, around 20–40 m, in exactly the locations where there are barrier layers present (Figure 14c), therefore also presenting the highly spatially variable pattern.

The event of barrier layer growth from February 14, 2009 to February 17, 2009 is illustrated in Figures 15 and 16. The 40 m thick barrier layer present on February 14, 2009 extending from 55°W to 53°W in this section along 17.69°N, grows to 60 m until February 17, 2009 due to dominantly a shallowing of the MLD during those 4 days (see dashed curves in Figures 15a, 16a, and 16b). The thinning of the mixed layer causes the BLT to be larger and is associated with a positive salinity vertical gradient tendency, meaning an increase in the salinity vertical gradient from 3 days before until the day of the peak BLT (Figure 15a). A similar, but weaker, pattern is seen in the temperature gradient tendency.

Looking at the individual contribution of salinity and temperature for the density stratification (Figures 16c–16e), it can be noticed that once again the MLD is mainly controlled by salinity, as the salinity stratification almost entirely match that of density. It can be also seen that the isohalines mostly move apart (stretch) and shift upwards during those 4 days (Figures 16a and 16b), which is the general case in 18/29 cases (62.1%).

Analyzing now the terms of the balance equations, the shifting upwards of the salinity gradient, seen in the tendency as a dipolar structure surrounding the MLD from February 14, 2009 (Figure 15a), can almost entirely be explained by horizontal advection (Figure 15c) and tilting (Figure 15g). Vertical advection and stretching are small and turbulent mixing of salinity acts to reduce the tilting and horizontal advection mechanisms. On the other hand, the temperature gradient tendency is entirely determined by horizontal advection, demonstrating that the tilting mechanism indeed is changing mostly salinity, since that is the variable possessing strong fronts in the region. So, despite the fact that evaporation exceeds river runoff and precipitation in this region (Figure 14h), there are thick barrier layers dominantly formed in this NEC region due to a tilting mechanism.

At the surface, there is northward horizontal advection of fresher waters from the Amazon river outflow and ITCZ precipitation by the NBC and associated rings, which are prevalent throughout the year and by equatorial divergence in fall and winter (Mignot et al., 2007). Indeed, Figure 14d shows the SSS and the currents at the surface pointing to a northwestward movement in the location of maximum BLT (Figure 14a). The Salinity Maximum Water (SMW) also exhibits a strong seasonality, with maximum subduction and export of the "salt river" toward the Caribbean Sea occurring in winter-spring (Blanke et al., 2002; Schmitt & Blair, 2015, Figure 4 in Qu et al., 2011). Blanke et al. (2002) pointed out that most of the flow from the center of the gyre enters the Caribbean Sea (8.2 Sv, 73%) and the peripheral salty water (1.1 Sv, 10%) reach 10°N. That means, the high salinity water is transported equatorward out of the formation domain in the subtropical gyre by the southwestward-oriented NEC.

In Figure 14f we see the large-scale southwestward flow and SMW spreading southwestward at 82.5 m which is a depth inside the ILD on this day. The saline water >37 psu is seen to penetrate the ILD depth range and in the process raise the MLD (Figures 16a and 16b). This explains the horizontal advection negative contribution to the salinity gradient tendency (Figures 15a and 15c). But a vertical shear is created when the southwestward moving SMW subducts and penetrates into the isothermal layer, and, above that, a fresher northward flow is present. The shear in turn promotes a tilting of the vertical salinity front, leading to the positive signal in the tendency term (Figures 15a and 15g).

Turbulent mixing of fresher water homogenizes the water column near the surface above MLD thus decreasing the salinity vertical gradient (Figure 15k), but below and at the MLD the turbulent mixing of the salinity increases the salinity gradient as the saltier water from below the MLD is entrained into the MLD, also reducing the MLD and contributing to the growth of BLT.

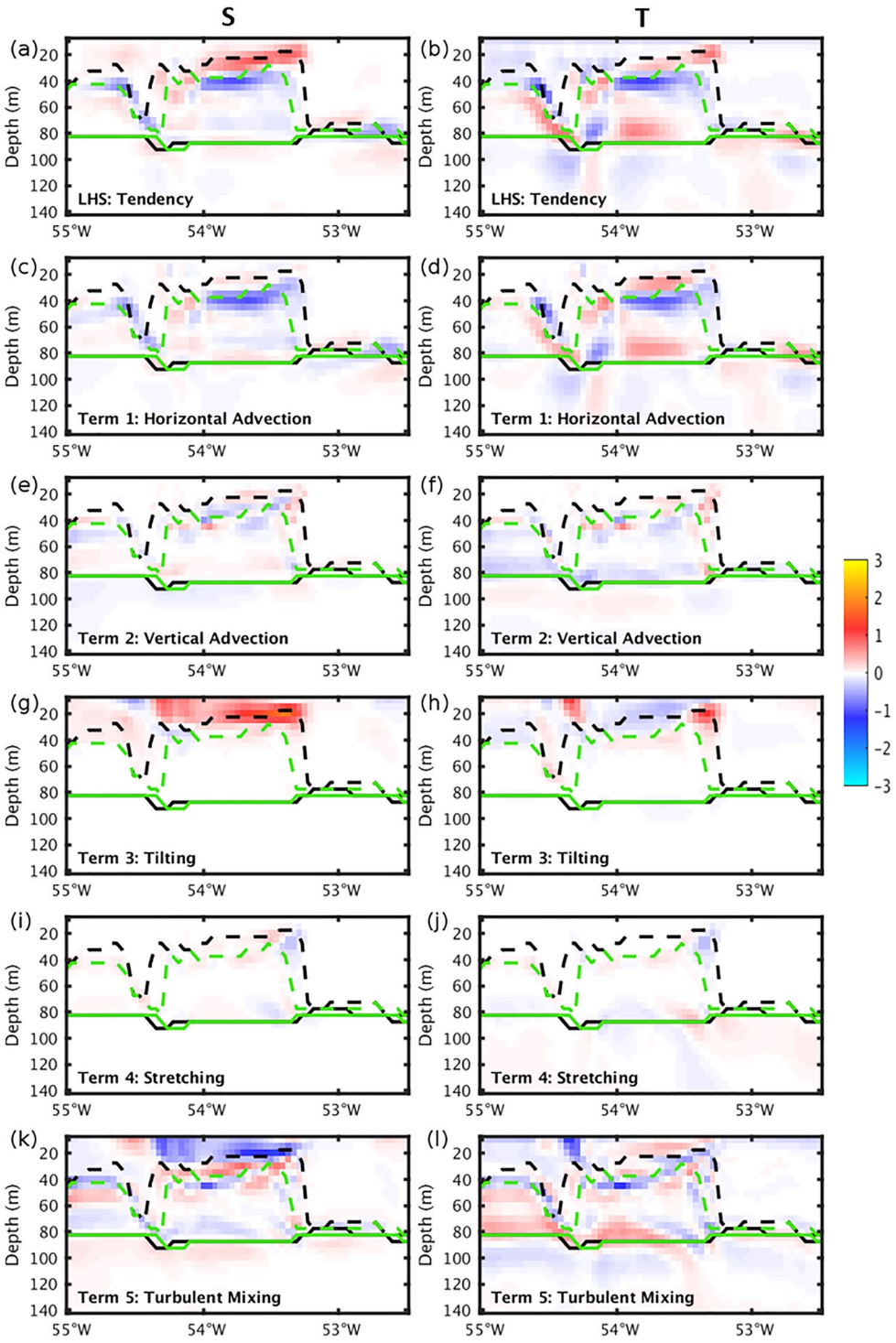

Figure 15. Vertical section at 17.69°N through the maximum BLT present on February 17, 2009 of salinity and temperature gradient balance terms: (a), (b) LHS; (c), (d) Term 1: Horizontal advection; (e), (f) Term 2: Vertical advection; (g), (h) Term 3: Tilting; (i), (j) Term 4: Stretching; (k), (l) Term 5: Turbulent mixing, averaged from February 14, 2009 to February 17, 2009 (units are $\times 10^{-7}$ psu/m.s and $\times 10^{-7}$°C/m.s, respectively). Black (green) solid lines correspond to the ILD, black (green) dashed lines correspond to the MLD for February 17, 2009 (February 14, 2009). BLT, barrier layer thickness; ILD, isothermal layer depth; MLD, mixed layer depth; LHS, left hand side.

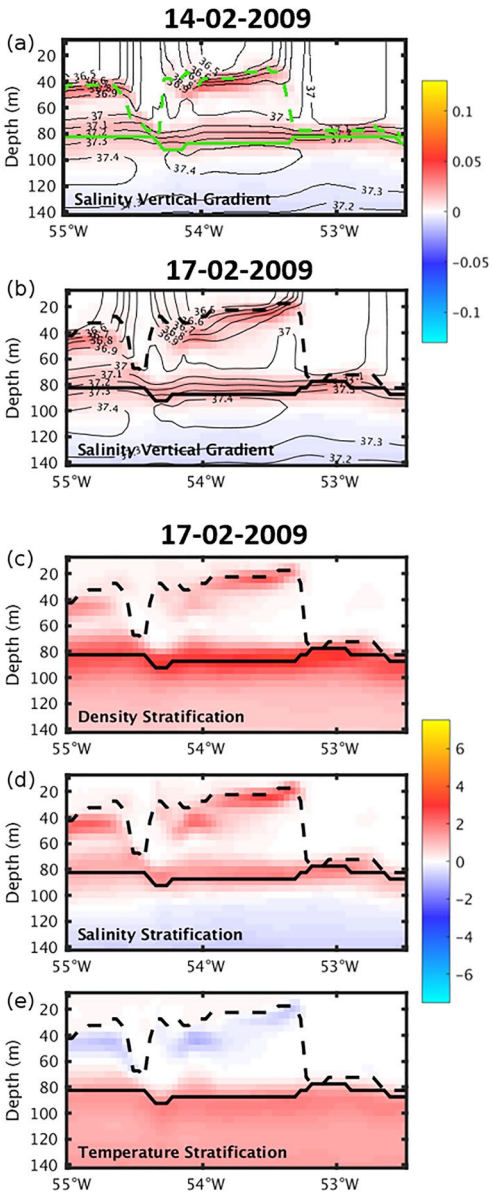

Figure 16. Vertical section at 17.69°N through the maximum BLT on February 17, 2009. Salinity vertical gradient (psu/m) with isohalines (psu) superimposed for (a) February 14, 2009 and (b) February 17, 2009. Density (c), salinity (d) and temperature (e) stratification ($\times 10^{-4}/s^2$) for February 17, 2009 are shown. Black (green) solid lines correspond to the ILD, black (green) dashed lines to the MLD for February 17, 2009 (February 14, 2009). BLT, barrier layer thickness; ILD, isothermal layer depth; MLD, mixed layer depth.

In conclusion, barrier layers in the NEC region are formed in an area of relatively uniform temperature, due to mainly tilting of salinity fronts. Barrier layers exist on the lower SSS side where the MLD is around 20 m adjacent to the higher SSS side where the MLD is around 90 m (Figures 14a, 14c and 14d). This is consistent with the results of Katsura et al. (2015) for the subtropical Pacific and Veneziani et al. (2014) for subtropical south Atlantic. If a strong shear does not exist above the ILD base due to a weaker northward flow in some areas, simply the convergence of the two water masses may also cause the salinity gradient to intensify. The heavy dense salty water could subduct into the isothermal layer at this region of convergence, thus also shoaling the MLD and forming a barrier layer. This process is explained by Vialard and Delecluse (1998) for barrier layers in the Pacific. In the total 36 events analyzed with our simulation, we found that the NEC BLT grew due to a shoaling of MLD with negligible or no change in ILD.

5.2.2. Barrier Layer Decay

In order to study the decay of the above described barrier layers, the average of the salinity and temperature gradient balance terms are now taken for the day of the peak BLT in each of the events encircled in the BLT time series and few days after the peak, when we see the barrier layer getting thinner.

In the shown case of January 06, 2006 (Figure 17), the mixed layer deepens during the course of the averaged 4 days (see depth change of black to green dashed curves). The pattern of salinity gradient tendency is now the opposite of the one seen before when analyzing the growth of BLT in the region. The deepening of the MLD is associated with a negative salinity vertical gradient tendency (blue in Figure 17a) above the resulting MLD (green curve) and below it to a positive tendency. This reveals a downward shift of the salinity gradient (see change from Figures 17g to 17h) and an increase in its magnitude. In fact this is happening in the majority of the cases identified (18/29 times, 62.1%).

As in the case of the barrier layer growth, the dominant terms contributing to the tendency are still horizontal advection and tilting (Figures 17b and 17d), but in the decay phase, turbulent mixing (Figure 17f) is fundamental. Tilting is now being completely counteracted by turbulent mixing, so that in the end the tendency above the MLD is negative.

In conclusion, we saw in this section that the BLT is maximum in the NEC region during the winter months of February-March and has a seasonal minimum in April-May. Tilting followed by stretching, horizontal advection and turbulent mixing are the dominant mechanisms that mostly stretch the isohalines to reduce the MLD, generating a barrier layer in this region. The barrier layers here decay mostly when the MLD deepens due to the compression and a downward shift of isohalines brought about by turbulent mixing and horizontal advection. On a seasonal perspective, the barrier layer grows due to slower deepening of MLD and comparatively faster deepening of ILD in winter and is completely eroded in spring by shoaling of ILD due to temperature stratification change. Specifically, during this increase in temperature stratification, there is compression of isotherms due to turbulent surface heat mixing (known from examining (not shown) the events in green in Figure 12).

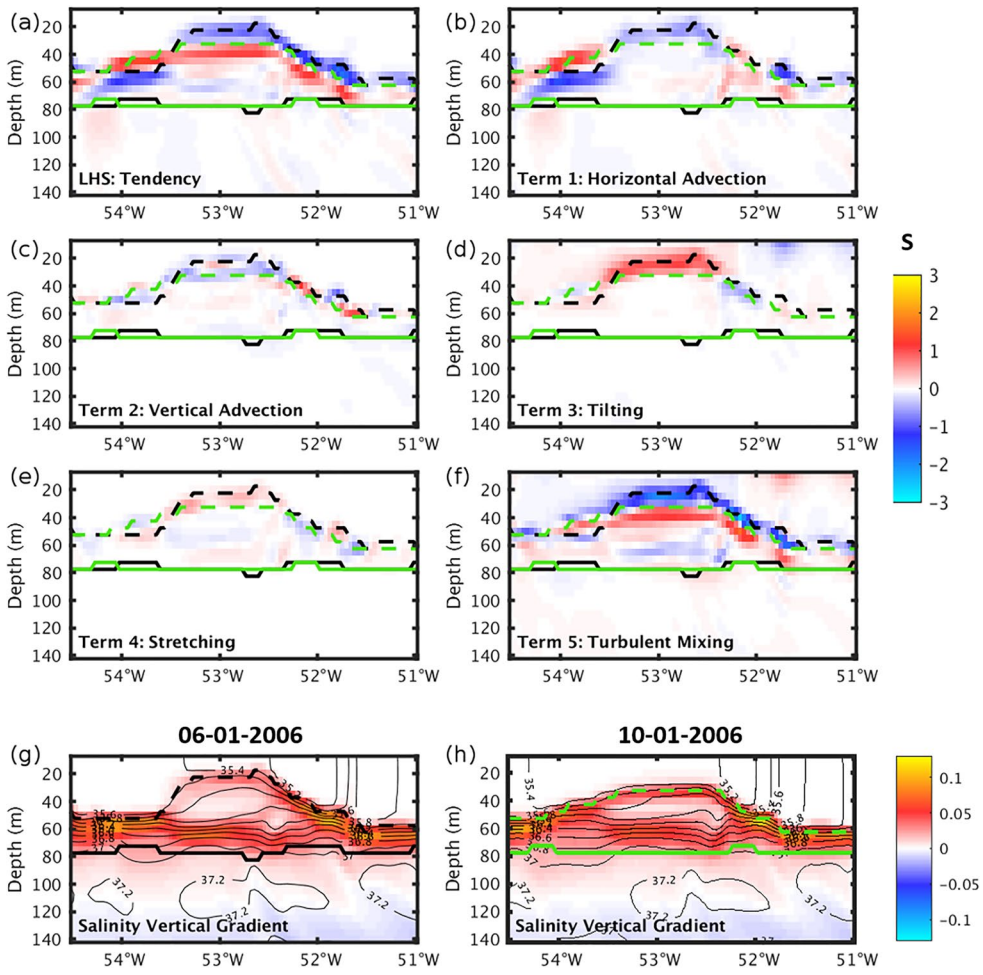

Figure 17. Vertical section at 14.23°N through the maximum BLT of January 06, 2006. Salinity gradient balance terms ($\times 10^{-7}$ psu/m.s) are averaged from January 06, 2006 to January 10, 2006. The salinity vertical gradient (psu/m) with isohalines (psu) superimposed are shown for (g) January 06, 2006 and (h) January 10, 2006. Black (green) solid lines correspond to the ILD, black (green) dashed lines to the MLD for January 06, 2006 (January 10, 2006).

6. Summary and Concluding Remarks

The results shown indicate that the northwestern tropical Atlantic has quasi-permanent barrier layers present in two localized regions: The NBC rings area and the region along the NEC, having different seasonality of barrier layers and different mechanisms behind their growth and decay.

In this study, the NBC rings have been identified to play a major role in advecting conditions that support the existence of barrier layers toward the northwest, by transporting freshwater originating from the Amazon and Orinoco rivers and from ITCZ precipitation. The dynamics intrinsic to the NBC rings and intrinsic to their formation, also are per se capable of growing barrier layers within the rings. All the NBC rings generated in the analyzed simulation have barrier layers either in their core or in their periphery during some period of their lifetime. According to our findings, the BLT is maximum in the ring's core and periphery in summer. There are thin barrier layers in the core and periphery of the rings in fall. The BLT in the NBC rings during winter is larger at the periphery than at the core of the ring.

The localized barrier layers larger than 80 m inside NBC rings during late June to July (summer) are mainly due to a deepening of the ILD by a stretching of the isotherms (Figure 10), caused by horizontal temperature advection, tilting of temperature fronts and stretching mechanisms. The decay of the BLT in the NBC rings is also mainly due to stretching of the isotherms (Figure 11) due to horizontal temperature advection,

stretching, tilting and turbulent mixing mechanisms which cause the ILD to reduce. The seasonal ILD increase in June to July in the NBC rings region is due to the reduction in the net heat flux forcing in the middle of increasing net heat forcing toward summer, causing a short period of reduction in SST, which brings about an increase in ILD which gets isolated in the NBC rings. Apart from that, the ILD increases and reduces moreover due to the internal eddy dynamics as explained above.

Amazon freshwater advected by NBC rings have been referred to before in Ffield (2007) but the barrier layers in those eddies were not studied. Overall, the occurring large summer BLT in NBC rings seems to be determined by changes in ILD rather than changes in MLD. This constitutes a novel finding in the present work.

The seasonal maximum in barrier layer presence in the NEC region further to the north is in winter and the minimum in spring (Figures 5b and 12), a result that is consistent with previous studies (Balaguru, Chang, Saravanan, & Jang, 2012; Breugem et al., 2008; Mignot et al., 2012; Sprintall & Tomczak, 1992). Winter convection and turbulent mixing cause the deepening of MLD and ILD in winter, but the rate of deepening of MLD is smaller than that of ILD. The largest barrier layers (>90 m) form and grow in winter during January to early March due to a reduction in MLD caused by stretching apart of the isohalines (Figure 16), over the deeper seasonal ILD. Tilting of salinity fronts caused by the northward and northwestward flow of fresh equatorial water at the surface by NBC, NBC eddies and Ekman currents, and the equatorward flow of the SMW at the subsurface "entering" into the isothermal layer, was identified to be dominant in the growth of barrier layers there (Figure 15). This corroborates recent studies by Katsura et al. (2015) and Katsura and Sprintall (2020), in which tilting of salinity fronts is suggested to be the main mechanism acting in the subtropical Pacific and eastern tropical north Pacific in forming the barrier layers there. In the subtropical Atlantic it was hypothesized earlier by Sprintall and Tomczak (1992) and Sato et al. (2006). Apart from tilting, we found that stretching, horizontal advection and turbulent mixing also contribute in the formation of the barrier layers in the NEC region.

It was found that the barrier layers in the NEC region get thin mainly because of compression and shifting down of isohalines (Figure 17), due to turbulent mixing and horizontal advection, which cause the mixed layer to deepen. The winter BLT is completely eroded in spring due to the shallowing of the isothermal and mixed layers by surface temperature stratification, a finding which corroborates results from (Mignot et al., 2012). The ILD shoals in spring by compression of isotherms due to turbulent mixing. In summer there is thin BLT due to the shoaling of MLD by again mainly tilting of salinity fronts and a slight deepening of ILD due to turbulent heat mixing. This thin BLT decays in September due to shoaling of the ILD. Overall, the formation and evolution of barrier layers in the NEC area is mostly depending on changes in the MLD.

We have seen that, in general, the magnitudes of all the mechanisms responsible for the growth and evolution of barrier layers are larger in the NBC rings in comparison to the magnitudes in the NEC region. This may be because the region south of 13°N close to the western boundary has higher magnitude of temperature and freshwater forcing and stronger western boundary currents and eddy dynamics. Also, there is stronger dynamics and gradients at the river plume edge. Second, though the seasonal cycles of the ILD and MLD are different in the different regions, it was seen that the reduction in net heat flux, forcing the SST, played an important role in cooling the surface and thus giving rise to convective mixing at the surface. This, along with mixing due to strong winds, caused the ILD and MLD to deepen. The semi-annual behavior of wind stress and of the net heat flux are important factors in determining the seasonal variability of ILD and MLD in both the regions in the western tropical Atlantic.

This work highlights that barrier layers are localized phenomena, which can form and grow at times solely because of ocean dynamics, such as surface and subsurface currents, subduction, fronts, eddies, and filaments, without the presence of a local surface freshwater influx. With the growing availability of comprehensive observations of ocean temperature, salinity and zonal, meridional and vertical currents, resolved spatially and in depth and also in coastal regions, it will be interesting to apply our findings from the simulation to observations. At present, it is only possible to study these detailed mechanisms of growth/decay in four dimensions with high resolution model outputs.

Our results give an insight into the mechanisms governing the formation, evolution and erosion of the quasi-permanent barrier layers in the western tropical Atlantic. Extending this study to a longer period

could enhance the robustness of our conclusions. The growth and decay mechanisms discussed here can be translated into other regions of the World Ocean, where similar physical conditions for barrier layer existence are prevalent, for example, in the subtropical and equatorial Pacific, in other river plume regions, other areas in the tropics which receive ITCZ rainfall and in farthest northern or southern latitudes where the freshwater influx is due to ice melt.

Data Availability Statement

The observational EN4.2.1 data set are available from the Met Office Hadley Center website (https://www.metoffice.gov.uk/hadobs/en4) and the barrier layer climatology is available from the IFREMER website (http://www.ifremer.fr/cerweb/deboyer/mld). The model results presented in this work can be retrieved from https://www.doi.org/10.5281/zenodo.4247363.

Acknowledgments
This work was performed in the framework of the German project "Atlantic Freshwater Cycle" (FOR1740), funded by the Deutsche Forschungsgemeinschaft (DFG). The model simulation was performed at the Deutsches Klimarechenzentrum (DKRZ), Hamburg, Germany under project 704. This is a contribution to the DFG funded Excellence Cluster CliCCS at the Center for Earth System Research and Sustainability (CEN) of the Universität Hamburg. Open access funding enabled and organized by Projekt DEAL.

References

Agarwal, N., Sharma, R., Parekh, A., Basu, S., Sarkar, A., & Agarwal, V. K. (2012). Argo observations of barrier layer in the tropical Indian Ocean. *Advances in Space Research*, *50*(5), 642–654. https://doi.org/10.1016/j.asr.2012.05.021

Balaguru, K., Chang, P., Saravanan, R., & Jang, C. J. (2012). The barrier layer of the Atlantic warmpool: Formation mechanism and influence on the mean climate. *Tellus A: Dynamic Meteorology and Oceanography*, *64*(1), 18162. https://doi.org/10.3402/tellusa.v64i0.18162

Balaguru, K., Chang, P., Saravanan, R., Leung, L. R., Xu, Z., Li, M., & Hsieh, J.-S. (2012). Ocean barrier layers' effect on tropical cyclone intensification. *Proceedings of the National Academy of Sciences*, *109*(36), 14343–14347. https://doi.org/10.1073/pnas.1201364109

Biri, S., Serra, N., Scharffenberg, M. G., & Stammer, D. (2016). Atlantic sea surface height and velocity spectra inferred from satellite altimetry and a hierarchy of numerical simulations. *Journal of Geophysical Research: Oceans*, *121*(6), 4157–4177. https://doi.org/10.1002/2015JC011503

Blanke, B., Arhan, M., Lazar, A., & Prévost, G. (2002). A lagrangian numerical investigation of the origins and fates of the salinity maximum water in the Atlantic. *Journal of Geophysical Research*, *107*(C10), 27-1–27-15. https://doi.org/10.1029/2002JC001318

Boyer, T., Levitus, S., Garcia, H., Locarnini, R. A., Stephens, C., & Antonov, J. (2005). Objective analyses of annual, seasonal, and monthly temperature and salinity for the World Ocean on a 0.25° grid. *International Journal of Climatology*, *25*(7), 931–945. https://doi.org/10.1002/joc.1173

Breugem, W.-P., Chang, P., Jang, C. J., Mignot, J., & Hazeleger, W. (2008). Barrier layers and tropical Atlantic SST biases in coupled GCMs. *Tellus A: Dynamic Meteorology and Oceanography*, *60*(5), 885–897. https://doi.org/10.1111/j.1600-0870.2008.00343.x

Camara, I., Kolodziejczyk, N., Mignot, J., Lazar, A., & Gaye, A. T. (2015). On the seasonal variations of salinity of the tropical A tlantic mixed layer. *Journal of Geophysical Research: Oceans*, *120*(6), 4441–4462. https://doi.org/10.1002/2015JC010865

Chelton, D. B., Schlax, M. G., & Samelson, R. M. (2011). Global observations of nonlinear mesoscale eddies. *Progress in Oceanography*, *91*(2), 167–216. https://doi.org/10.1016/j.pocean.2011.01.002

Coles, V. J., Brooks, M. T., Hopkins, J., Stukel, M. R., Yager, P. L., & Hood, R. R. (2013). The pathways and properties of the Amazon river plume in the tropical north Atlantic Ocean. *Journal of. Geophysical Research: Oceans*, *118*(12), 6894–6913. https://doi.org/10.1002/2013JC008981

Cronin, M. F., & McPhaden, M. J. (2002). Barrier layer formation during westerly wind bursts. *Journal of Geophysical Research*, *107*(C12), SRF21-1–SRF21-12. https://doi.org/10.1029/2001JC001171

Da-Allada, C. Y., Alory, G., du Penhoat, Y., Kestenare, E., Durand, F., & Hounkonnou, N. M. (2013). Seasonal mixed-layer salinity balance in the tropical Atlantic Ocean: Mean state and seasonal cycle. *Journal of Geophysical Research: Oceans*, *118*(1), 332–345. https://doi.org/10.1029/2012JC008357

de Boyer Montégut, C., Madec, G., Fischer, A. S., Lazar, A., & Iudicone, D. (2004). Mixed layer depth over the global ocean: An examination of profile data and a profile-based climatology. *Journal of Geophysical Research*, *109*(C12). https://doi.org/10.1029/2004JC002378

de Boyer Montégut, C., Mignot, J., Lazar, A., & Cravatte, S. (2007). Control of salinity on the mixed layer depth in the world ocean: 1. General description. *Journal of Geophysical Research*, *112*(C6). https://doi.org/10.1029/2006JC003953

Dee, D. P., Uppala, S. M., Simmons, A. J., Berrisford, P., Poli, P., Kobayashi, S., et al. (2011). The ERA-Interim reanalysis: Configuration and performance of the data assimilation system. *Quarterly Journal of the Royal Meteorological Society*, *137*(656), 553–597. https://doi.org/10.1002/qj.828

Drushka, K., Sprintall, J., & Gille, S. T. (2014). Subseasonal variations in salinity and barrier-layer thickness in the eastern equatorial Indian Ocean. *Journal of Geophysical Research: Oceans*, *119*(2), 805–823. https://doi.org/10.1002/2013JC009422

Ferry, N., & Reverdin, G. (2004). Sea surface salinity interannual variability in the western tropical Atlantic: An ocean general circulation model study. *Journal of Geophysical Research*, *109*(C5). https://doi.org/10.1029/2003JC002122

Ffield, A. (2007). Amazon and Orinoco river plumes and NBC rings: Bystanders or participants in hurricane events?. *Journal of Climate*, *20*(2), 316–333. https://doi.org/10.1175/JCLI3985.1

Foltz, G. R., Grodsky, S. A., Carton, J. A., & McPhaden, M. J. (2004). Seasonal salt budget of the northwestern tropical Atlantic Ocean along 38°W. *Journal of Geophysical Research*, *109*(C3). https://doi.org/10.1029/2003JC002111

Foltz, G. R., & McPhaden, M. J. (2008). Seasonal mixed layer salinity balance of the tropical north Atlantic Ocean. *Journal of Geophysical Research*, *113*(C2). https://doi.org/10.1029/2007JC004178

Fonseca, C. A., Goni, G. J., Johns, W. E., & Campos, E. J. D. (2004). Investigation of the north Brazil Current retroflection and north equatorial countercurrent variability. *Geophysical Research Letters*, *31*. https://doi.org/10.1029/2004GL020054

Fournier, S., Vandemark, D., Gaultier, L., Lee, T., Jonsson, B., & Gierach, M. M. (2017). Interannual variation in offshore advection of Amazon-Orinoco plume waters: Observations, forcing mechanisms, and impacts. *Journal of Geophysical Research: Oceans*, *122*(11), 8966–8982. https://doi.org/10.1002/2017JC013103

Fratantoni, D. M., & Glickson, D. A. (2002). North Brazil Current ring generation and evolution observed with SeaWiFS. *Journal of Physical Oceanography*, *32*(3), 1058–1074. https://doi.org/10.1175/1520-0485(2002)032<1058:NBCRGA>2.0.CO;2

Fratantoni, D. M., Johns, W. E., Townsend, T. L., & Hurlburt, H. E. (2000). Low-latitude circulation and mass transport pathways in a model of the tropical Atlantic Ocean. *Journal of Physical Oceanography*, *30*(8), 1944–1966. https://doi.org/10.1175/1520-0485(2000)030<1944:LLCAMT>2.0.CO;2

Fratantoni, D. M., & Richardson, P. L. (2006). The evolution and demise of north Brazil Current rings. *Journal of Physical Oceanography*, *36*(7), 1241–1264. https://doi.org/10.1175/JPO2907.1

Good, S. A., Martin, M. J., & Rayner, N. A. (2013). EN4: Quality controlled ocean temperature and salinity profiles and monthly objective analyses with uncertainty estimates. *Journal of Geophysical Research: Oceans*, *118*(12), 6704–6716. https://doi.org/10.1002/2013JC009067

Gouretski, V., & Reseghetti, F. (2010). On depth and temperature biases in bathythermograph data: Development of a new correction scheme based on analysis of a global ocean database. *Deep Sea Research Part I: Oceanographic Research Papers*, *57*(6), 812–833. https://doi.org/10.1016/j.dsr.2010.03.011

Hellweger, F. L., & Gordon, A. L. (2002). Tracing Amazon river water into the Caribbean Sea. *Journal of Marine Research*, *60*(4), 537–549. https://doi.org/10.1357/002224002762324202

Isern-Fontanet, J., Font, J., García-Ladona, E., Emelianov, M., Millot, C., & Taupier-Letage, I. (2004). Spatial structure of anticyclonic eddies in the Algerian basin (Mediterranean Sea) analyzed using the Okubo-Weiss parameter. *Deep Sea Research Part II: Topical Studies in Oceanography*, *51*, 3009–3028. https://doi.org/10.1016/j.dsr2.2004.09.013

Jochum, M., & Malanotte-Rizzoli, P. (2003). On the generation of North Brazil Current rings. *Journal of Marine Research*, *61*(2), 147–173. https://doi.org/10.1357/002224003322005050

Katsura, S., Oka, E., & Sato, K. (2015). Formation mechanism of barrier layer in the subtropical Pacific. *Journal of Physical Oceanography*, *45*, 2790–2805. https://doi.org/10.1175/JPO-D-15-0028.1

Katsura, S., & Sprintall, J. (2020). Seasonality and formation of barrier layers and associated temperature inversions in the eastern tropical north Pacific. *Journal of Physical Oceanography*, *50*(3), 791–808. https://doi.org/10.1175/JPO-D-19-0194.1

Köhl, A., & Serra, N. (2014). Causes of decadal changes of the freshwater content in the Arctic Ocean. *Journal of Climate*, *27*(9), 3461–3475. https://doi.org/10.1175/JCLI-D-13-00389.1

Koldunov, N. V., Serra, N., Köhl, A., Stammer, D., Henry, O., Cazenave, A., et al. (2014). Multimodel simulations of Arctic Ocean sea surface height variability in the period 1970–2009. *Journal of Geophysical Research: Oceans*, *119*(12), 8936–8954. https://doi.org/10.1002/2014JC010170

Liu, H., Wang, C., Lee, S.-K., & Enfield, D. (2012). Atlantic warm-pool variability in the IPCC AR4 CGCM simulations. *Journal of Climate*, *25*(16), 5612–5628. https://doi.org/10.1175/JCLI-D-11-00376.1

Maes, C., & O'Kane, T. J. (2014). Seasonal variations of the upper ocean salinity stratification in the Tropics. *Journal of Geophysical Research: Oceans*, *119*(3), 1706–1722. https://doi.org/10.1002/2013JC009366

Marshall, J., Adcroft, A., Hill, C., Perelman, L., & Heisey, C. (1997). A finite-volume, incompressible Navier Stokes model for studies of the ocean on parallel computers. *Journal of Geophysical Research*, *102*(C3), 5753–5766. https://doi.org/10.1029/96JC02775

Masson, S., & Delecluse, P. (2001). Influence of the Amazon river runoff on the tropical Atlantic. *Physics and Chemistry of the Earth, Part B: Hydrology, Oceans and Atmosphere*, *26*(2), 137–142. https://doi.org/10.1016/S1464-1909(00)00230-6

Mignot, J., de Boyer Montégut, C., Lazar, A., & Cravatte, S. (2007). Control of salinity on the mixed layer depth in the world ocean: 2. Tropical areas. *Journal of Geophysical Research*, *112*(C10). https://doi.org/10.1029/2006JC003954

Mignot, J., Lazar, A., & Lacarra, M. (2012). On the formation of barrier layers and associated vertical temperature inversions: A focus on the northwestern tropical Atlantic. *Journal of Geophysical Research*, *117*(C2). https://doi.org/10.1029/2011JC007435

Pailler, K., Bourlès, B., & Gouriou, Y. (1999). The barrier layer in the western tropical Atlantic Ocean. *Geophysical Research Letters*, *26*(14), 2069–2072. https://doi.org/10.1029/1999GL900492

Pan, L., Zhong, Y., Liu, H., Zhou, L., Zhang, Z., & Zhou, M. (2018). Seasonal variation of barrier layer in the Southern Ocean. *Journal of Geophysical Research: Oceans*, *123*(3), 2238–2253. https://doi.org/10.1002/2017JC013382

Qu, T., Gao, S., & Fukumori, I. (2011). What governs the North Atlantic salinity maximum in a global GCM?. *Geophysical Research Letters*, *38*(7). https://doi.org/10.1029/2011GL046757

Rudzin, J. E., Shay, L. K., Jaimes, B., & Brewster, J. K. (2017). Upper ocean observations in eastern Caribbean Sea reveal barrier layer within a warm core eddy. *Journal of Geophysical Research: Oceans*, *122*(2), 1057–1071. https://doi.org/10.1002/2016JC012339

Sato, K., Suga, T., & Hanawa, K. (2006). Barrier layers in the subtropical gyres of the world's oceans. *Geophysical Research Letters*, *33*(8). https://doi.org/10.1029/2005GL025631

Schiller, R. V., & Smith, R. B. (2018). On extreme surface and sub-surface currents driven by North Brazil Current rings offshore Suriname. *Paper presented at the Offshore Technology Conference*. https://doi.org/10.4043/29023-MS

Schmitt, R., Blair, A., & Blair, A. (2015). A river of salt. *Oceanography*, *28*(1), 40–45. https://doi.org/10.5670/oceanog.2015.04

Schott, F. A., Fischer, J., & Stramma, L. (1998). Transports and pathways of the upper-layer circulation in the western tropical Atlantic. *Journal of Physical Oceanography*, *28*(10), 1904–1928. https://doi.org/10.1175/1520-0485(1998)028<1904:TAPOTU>2.0.CO;2

Sena Martins, M., Serra, N., & Stammer, D. (2015). Spatial and temporal scales of sea surface salinity variability in the Atlantic Ocean. *Journal of Geophysical Reserach: Oceans*, *120*(6), 4306–4323. https://doi.org/10.1002/2014JC010649

Serra, N., Käse, R. H., Köhl, A., Stammer, D., & Quadfasel, D. (2010). On the low-frequency phase relation between the Denmark Strait and the Faroe-Bank Channel overflows. *Tellus*, *62*(4), 530–550. https://www.tandfonline.com/doi/abs/10.1111/j.1600-0870.2009.00445.x

Silva, A., Araujo, M., Medeiros, C., Silva, M., & Bourlès, B. (2005). Seasonal changes in the mixed and barrier layers in the western equatorial Atlantic. *Brazilian Journal of Oceanography*, *53*(3–4), 83–98. https://doi.org/10.1590/S1679-87592005000200001

Sommer, A., Reverdin, G., Kolodziejczyk, N., & Boutin, J. (2015). Sea surface salinity and temperature budgets in the north Atlantic subtropical gyre during SPURS experiment: August 2012–August 2013. *Frontiers in Marine Science*, *2*, 107. https://doi.org/10.3389/fmars.2015.00107

Sprintall, J., & Tomczak, M. (1992). Evidence of the barrier layer in the surface layer of the tropics. *Journal of Geophysical Research*, *97*(C5), 7305–7316. https://doi.org/10.1029/92JC00407

Stramma, L., Rhein, M., Brandt, P., Dengler, M., Böning, C., & Walter, M. (2005). Upper ocean circulation in the western tropical Atlantic in boreal fall 2000. *Deep Sea Research Part I: Oceanographic Research Papers*, *52*(2), 221–240. https://doi.org/10.1016/j.dsr.2004.07.021

van der Boog, C. G., Pietrzak, J. D., Dijkstra, H. A., Brüggemann, N., van Westen, R. M., James, R. K., et al. (2019). The impact of upwelling on the intensification of anticyclonic ocean eddies in the Caribbean Sea. *Ocean Science*, *15*(6), 1419–1437. https://doi.org/10.5194/os-15-1419-2019

Varona, H. L., Veleda, D., Silva, M., Cintra, M., & Araujo, M. (2019). Amazon river plume influence on western tropical Atlantic dynamic variability. *Dynamics of Atmospheres and Oceans*, *85*, 1–15. https://doi.org/10.1016/j.dynatmoce.2018.10.002

Veneziani, M., Griffa, A., Garraffo, Z., & Mensa, J. A. (2014). Barrier layers in the tropical south Atlantic: Mean dynamics and submesoscale effects. *Journal of Physical Oceanography*, *44*(1), 265–288. https://doi.org/10.1175/JPO-D-13-064.1

Vialard, J., & Delecluse, P. (1998). An OGCM study for the TOGA decade. Part II: Barrier-layer formation and variability. *Journal of Physical Oceanography*, *28*(6), 1089–1106. https://doi.org/10.1175/1520-0485(1998)028<1089:AOSFTT>2.0.CO;2